doi.org/10.36721/PJPS/2026.40.14705.1

Determination of cytotoxic effect of *Curcuma longa* extract on MDA-MB-231 and MCF-10A cell lines

Hanzla Arshad[1,2]*, Inaam Ur Rehman[3], Muhammad Muneeb[3], Aiman Mahmood[4], Abdul Rehman Riaz[4] and Saif Ullah Khan[4]

[1]Punjab University College of Pharmacy, University of the Punjab, Lahore, Pakistan
[2]Veterinary Research Institute, Zarrar Shaheed Road, Cantt, Lahore, Pakistan
[3]Yashfeen College of Pharmacy, Yashfeen Education System, Lahore, Pakistan
[4]Lecturer, Department of Pharmacy, University of Rasul, Mandi Bahauddin, Punjab, Pakistan
[5]Department of Pharmacy, Minhaj University, Lahore, Pakistan

Abstract: **Background**: Breast cancer therapy is limited by drug resistance and systemic toxicity. *Curcuma longa* contains hydrophobic curcuminoids with reported anticancer activity. **Objectives**: The study evaluated the cytotoxic and apoptosis-inducing effect of dichloromethane extract of *Curcuma longa* on MDA-MB-231 breast cancer cells and MCF-10A non-tumourigenic mammary epithelial cells. **Methods**: *Curcuma longa* rhizomes were extracted with dichloromethane. Chemical profiling was performed by high-performance liquid chromatography, liquid chromatography-mass spectrometry and Fourier-transform infrared spectroscopy. MDA-MB-231 and MCF-10A cells were treated with *Curcuma longa* extract or doxorubicin. Cell viability was assessed by MTT assay. Trypan blue, phase-contrast microscopy, Annexin V/propidium iodide staining, Hoechst/propidium iodide staining, reactive oxygen species assay, wound-healing assay, lactate dehydrogenase assay, JC-1 assay, caspase-3/7 and caspase-9 assays and reverse transcription quantitative polymerase chain reaction were used to assess cytotoxicity, apoptosis, oxidative stress, mitochondrial damage and gene-expression changes. **Results**: *Curcuma longa* extract reduced MDA-MB-231 viability in a dose-dependent manner and showed limited toxicity toward MCF-10A cells. The IC_{50} was 18.50 µg mL^{-1} in MDA-MB-231 cells and remained above 256 µg mL^{-1} in MCF-10A cells. The extract increased reactive oxygen species levels, lactate dehydrogenase release, mitochondrial depolarisation and caspase activity in cancer cells. It also increased BAX and CASP9 expression and reduced BCL2 and TOP2A expression. Chemical analysis confirmed curcumin, demethoxycurcumin and bisdemethoxycurcumin. **Conclusion**: Dichloromethane extract of *Curcuma longa* showed selective anticancer activity against MDA-MB-231 cells through oxidative stress and mitochondria-mediated apoptosis.

Keywords: Apoptosis; Breast cancer; *Curcuma longa*; Cytotoxicity; Reactive oxygen species.

Submitted 03-06-2025 – Revised 21-10-2025 – Accepted 07-11-2025

Article in Press

INTRODUCTION

Breast cancer remains the most frequently diagnosed malignancy in women and a leading cause of cancer-related death worldwide (Bray *et al*., 2024). Its incidence continues to rise in many regions and survival gains remain uneven across countries and molecular subtypes. Standard therapeutic approaches, including surgery, radiotherapy, endocrine therapy, targeted agents and cytotoxic chemotherapy, have improved clinical outcomes. However, intrinsic or acquired drug resistance, systemic toxicity and treatment-related quality-of-life impairment continue to limit their overall effectiveness (Lyon *et al*., 2022). These challenges underscore the need for agents that can suppress cancer cell growth while causing minimal damage to non-tumorigenic cells (Tufail *et al*., 2022).

Curcuma longa (CL), commonly known as turmeric, contains several bioactive constituents, including curcuminoids and non-polar compounds that can be extracted using organic solvents (Ye *et al*., 2012). Dichloromethane (DCM) extracts concentrate many hydrophobic constituents and have demonstrated antiproliferative and pro-apoptotic activities across various cancer models (Zhou *et al*., 2017; Nadeem *et al*., 2025). Reported mechanisms include induction of reactive oxygen species (ROS), mitochondrial dysfunction, modulation of B-cell lymphoma 2 (BCL2) family signaling, caspase activation and interference with cell-cycle and deoxyribonucleic acid (DNA) topology regulators. These multiple biological actions suggest that CL may act through more than one pathway and may offer a different toxicity profile from conventional chemotherapy.

The current study evaluates DCM extract of CL as an anticancer candidate in breast cancer models, using doxorubicin (DOX) as a clinically relevant comparator. The central hypothesis is that CL induces intrinsic, mitochondria-mediated apoptosis in cancer cells more strongly than DOX at matched concentrations, while exerting limited effects on non-tumorigenic mammary epithelial cells. To test this hypothesis, the study integrates complementary functional and molecular assays in MDA-MB-231 breast cancer cells and MCF-10A non-tumorigenic mammary epithelial cells.

**Corresponding author:* e-mail: hanzalaarshadbutt@gmail.com

Cell viability was assessed using the 3-(4,5-dimethylthiazol-2-yl)-2,5-diphenyltetrazolium bromide (MTT) assay, while membrane damage was evaluated through lactate dehydrogenase (LDH) release. Mitochondrial involvement was examined using 5,5′,6,6′-tetrachloro-1,1′,3,3′-tetraethylbenzimidazolylcarbocyanine iodide (JC-1) staining to assess mitochondrial membrane potential (ΔΨm). Initiator and executioner caspase activities were quantified using colorimetric assays for caspase-9 and caspase-3/7. Transcriptional responses were evaluated by reverse transcription quantitative polymerase chain reaction (RT-qPCR) for BCL2-associated X apoptosis regulator (*BAX*), *BCL2*, caspase-9 (*CASP9*) and topoisomerase II alpha (*TOP2A*) to examine apoptosis-related and proliferation-linked changes. Wound-healing and ROS assays were also included to place the apoptotic response within a broader stress-response and migration-related context (Abdulazeez *et al*., 2022). Chemical characterization was performed using Fourier-transform infrared spectroscopy (FT-IR), high-performance liquid chromatography (HPLC) and liquid chromatography-mass spectrometry (LC-MS) to document the composition of the CL extract. Side-by-side comparisons with DOX across 20, 40 and 80 µg mL^{-1} enabled assessment of dose response and selectivity. Statistical analyses included appropriate multiple-comparison control to support robust interpretation of the experimental findings (Vardhini *et al*., 2023). By combining functional assays, gene expression analysis and chemical profiling, the study aims to determine whether CL can induce cancer-selective apoptosis with a mechanistic pattern consistent with mitochondrial involvement. The findings may guide future bioactivity-guided fractionation, optimization and combination studies aimed at improving anticancer activity while reducing the limitations associated with standard anthracycline therapy. A graphical overview of the study design and experimental workflow is presented in fig. 1.

MATERIALS AND METHODS

Study design and experimental groups

An *in-vitro* experimental study was conducted to evaluate the cytotoxic, pro-apoptotic and cancer-selective effects of DCM extract of CL on MDA-MB-231 breast cancer cells and MCF-10A non-tumorigenic mammary epithelial cells. DOX was used as the positive comparator. For mechanistic assays, cells were treated with CL extract or DOX at 20, 40 and 80 µg mL^{-1} for 24 h. For half-maximal inhibitory concentration (IC_{50}) estimation by MTT assay, a wider two-fold concentration range of 8, 16, 32, 64, 128 and 256 µg mL^{-1} was used. Vehicle-treated cells served as negative controls. The final dimethyl sulfoxide (DMSO) concentration in CL-treated wells did not exceed 0.1% v/v. All experiments were performed in triplicate and repeated at least three times independently unless stated otherwise.

Chemicals and reagents

DCM (American Chemical Society [ACS] reagent, ≥99.5%, Cat. No. D65100), methanol (HPLC grade, ≥99.9%, Cat. No. 439193), ethanol absolute (≥99.8%, suitable for HPLC, Cat. No. 34852-M), acetone (HPLC grade, ≥99.9%, Cat. No. 270725), chloroform (ACS reagent, ≥99.8%, Cat. No. 319988), acetonitrile (HPLC and gas chromatography grade, ≥99.8%, Cat. No. 34881), glacial acetic acid (ACS reagent, ≥99.7%, Cat. No. 695092), hydrochloric acid (37%, ACS reagent, Cat. No. 258148), DMSO (sterile-filtered, Cat. No. D2650), phosphate-buffered saline (PBS) tablets (Cat. No. P4417), trypsin-ethylenediaminetetraacetic acid (EDTA) solution (0.25%, sterile-filtered, Cat. No. T4049), MTT reagent (Cat. No. M5655), trypan blue solution (0.4%, sterile-filtered, Cat. No. T8154), Hoechst 33342 (Cat. No. B2261), propidium iodide (PI) solution (1.0 mg mL^{-1} in water, Cat. No. P4864), JC-1 (Cat. No. T4069), carbonyl cyanide 3-chlorophenylhydrazone (CCCP; Cat. No. C2759), Triton X-100 (Cat. No. 648462), 2′,7′-dichlorodihydrofluorescein diacetate (DCFH-DA; Cat. No. D6883), curcumin analytical standard (Cat. No. 08511), demethoxycurcumin (Cat. No. D7696), bisdemethoxycurcumin reference material (Cat. No. PHR3434) and DOX (Cat. No. D1515) were obtained from Sigma-Aldrich/Merck.

Dulbecco's Modified Eagle's Medium (DMEM), high glucose, sterile-filtered and suitable for cell culture (Cat. No. D5796), DMEM/F-12 medium (Cat. No. D6421), fetal bovine serum (FBS; Cat. No. F7524), horse serum (Cat. No. H1270), penicillin-streptomycin solution (Cat. No. P4333), human epidermal growth factor (Cat. No. E9644), human insulin solution (Cat. No. I9278), hydrocortisone (Cat. No. H0888) and cholera toxin from *Vibrio cholerae* (Cat. No. C8052) were also obtained from Sigma-Aldrich/Merck. Annexin V-fluorescein isothiocyanate (FITC) Apoptosis Detection Kit (Cat. No. APOAF), Caspase 3 Assay Kit, Colorimetric (Cat. No. CASP3C) and Caspase-9 Colorimetric Activity Assay Kit (Cat. No. APT173) were obtained from Sigma-Aldrich/Merck. LDH release was measured using CytoTox-ONE™ Homogeneous Membrane Integrity Assay (Promega Corporation, Madison, WI, USA; Cat. No. G7890). Total ribonucleic acid (RNA) was isolated using TRIzol™ Reagent (Invitrogen/Thermo Fisher Scientific, Waltham, MA, USA; Cat. No. 15596026). Residual genomic DNA was removed using DNase I, RNase-free (Thermo Fisher Scientific, Cat. No. EN0521). Complementary DNA (cDNA) was synthesised using iScript™ cDNA Synthesis Kit (Bio-Rad Laboratories, Hercules, CA, USA; Cat. No. 1708891). RT-qPCR was performed using SsoAdvanced™ Universal SYBR® Green Supermix (Bio-Rad Laboratories; Cat. No. 1725271). Protein concentration was determined using Pierce™ bicinchoninic acid (BCA) Protein Assay Kit (Thermo Fisher Scientific; Cat. No. 23227).

Article in Press

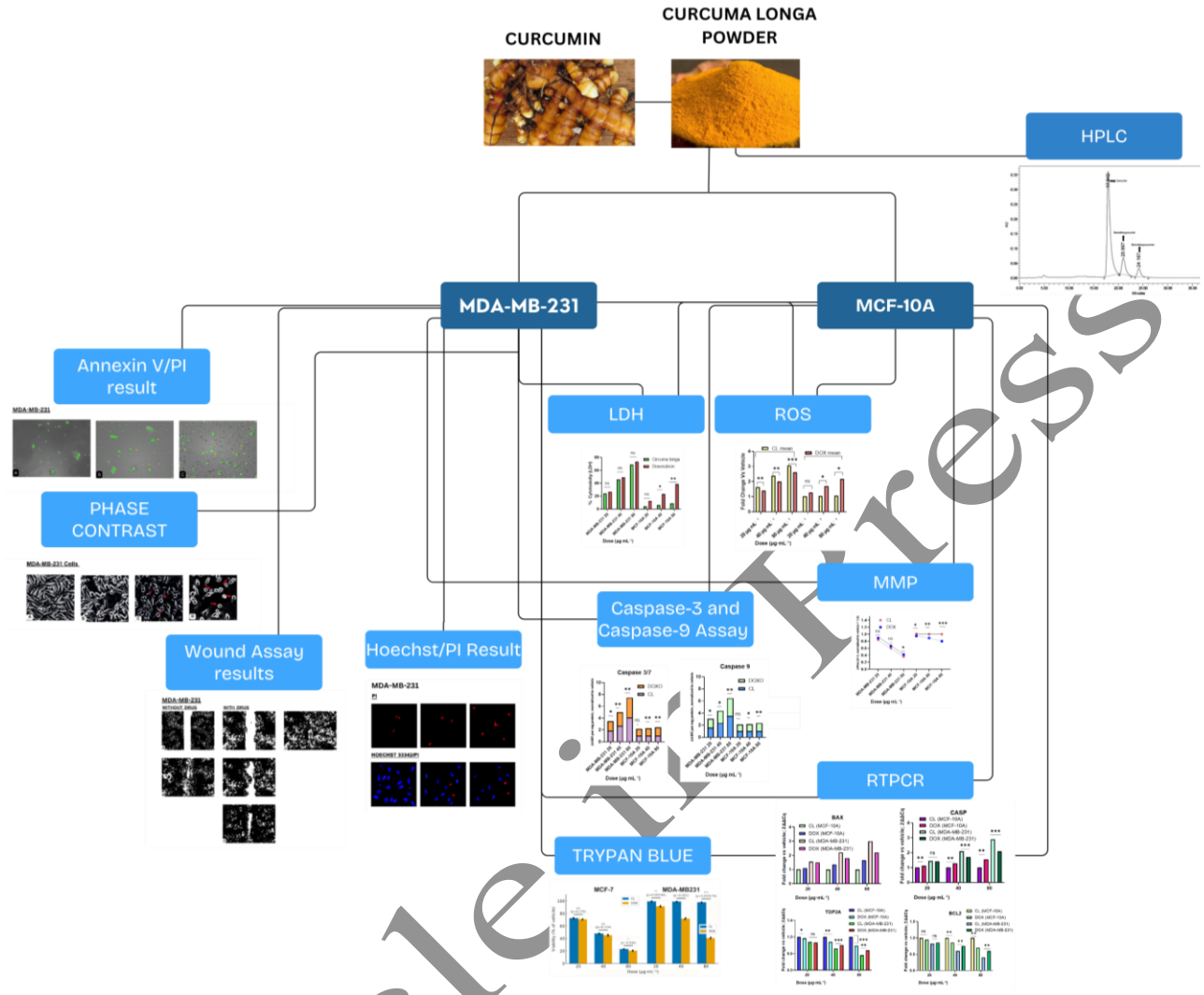


Fig. 1: Graphical abstract of the study.

Apparatus and equipment

Cell culture procedures were performed in an Airstream AC2-4S8 Class II Type A2 biosafety cabinet (Esco Lifesciences, Singapore). Cells were incubated in an MCO-170AC-PE IncuSafe carbon dioxide incubator (PHCbi/PHC Corporation, Japan) at 37°C with 5% carbon dioxide. Cell counting and viability assessment were performed using a CellDrop FL automated cell counter (DeNovix Inc., Wilmington, DE, USA; serial number S111-00). Morphological examination was carried out using a CKX53 inverted cell culture microscope (Evident/Olympus, Japan). Fluorescence-based imaging for Annexin V/PI and Hoechst 33342/PI staining was performed using a CKX53 fluorescence-equipped inverted microscope (Evident/Olympus, Japan). Solvent evaporation was performed in a Frontier Acela EFA-4UDRVW-8 ducted fume hood (Esco Lifesciences, Singapore). Extract drying was carried out using a Heratherm OMS60 General Protocol Oven (Thermo Fisher Scientific, Waltham, MA, USA). Solubility samples were mixed using a BenchMixer BV1000 vortex mixer (Benchmark Scientific, USA) and sonicated in an Elmasonic S 30 H ultrasonic bath (Elma Schmidbauer GmbH, Germany). Acid hydrolysis for chromatographic analysis was performed using a Precision GP 10 general-purpose water bath (Thermo Fisher Scientific, Waltham, MA, USA). Cell pellets and lysates were centrifuged using a refrigerated Centrifuge 5810 R (Eppendorf, Hamburg, Germany). Absorbance in the MTT assay was measured using an RT-6000 microplate reader (Rayto Life and Analytical Sciences, Shenzhen, China). ROS fluorescence was measured using a Varioskan ALF multimode microplate reader (Thermo Fisher Scientific, Waltham, MA, USA). LDH release and caspase activity were measured using an Infinite M1000 Pro microplate reader (Tecan, Männedorf, Switzerland). RNA concentration and purity were assessed using a NanoDrop One microvolume ultraviolet-visible spectrophotometer (Thermo Fisher Scientific, Waltham, MA, USA). RT-qPCR was performed using a CFX96 detection system (Bio-Rad Laboratories,

Article in Press

Hercules, CA, USA). FT-IR was performed using a Nicolet iS5 FT-IR spectrometer (Thermo Fisher Scientific, Waltham, MA, USA). HPLC was carried out using a Shimadzu LC-10A system (Shimadzu Corporation, Kyoto, Japan) equipped with an ultraviolet-visible detector and a Shim-pack CLC-ODS C18 column. LC-MS was performed using the same chromatographic system coupled to a QTRAP 4500 tandem mass spectrometry system (Sciex, Framingham, MA, USA) equipped with an electrospray ionisation source. Wound area was quantified using ImageJ software version 1.54t.

Preparation of CL extract

Fresh CL rhizomes were washed under running tap water for 30 min and then rinsed repeatedly with distilled water to remove adhering soil and surface contaminants. The cleaned rhizomes were cut into small pieces and shade-dried at room temperature until surface moisture was removed. A total of 241.24 g of chopped plant material was transferred into a clean one-liter glass bottle and macerated with 500 mL of DCM for five days at room temperature. The bottle was sealed and shaken intermittently during maceration to improve solvent contact with the plant material. The extraction procedure was adapted from standard solvent maceration methods used for medicinal plants (Azwanida, 2015). After maceration, the mixture was filtered through Whatman No. 1 filter paper. The filtrate was kept in the ducted fume hood until the DCM evaporated. The semi-solid residue was transferred into a clean Petri dish and dried in the hot-air oven at 40°C until a dry powder was obtained. The dried extract was weighed to calculate percentage yield, transferred into an airtight amber container and stored at 4°C until further use. For biological assays, 20 mg of dried CL extract was dissolved in 1 mL DMSO to prepare a 20 mg mL^{-1} stock solution. The stock solution was filtered through a sterile 0.22 µm syringe filter before use in cell culture experiments.

Solubility analysis

The qualitative solubility of the dried DCM extract of CL was evaluated in distilled water, chloroform, acetone, ethanol and methanol using a room-temperature solvent-screening procedure, with the visual classification criteria adapted from Altundag *et al*. (2025). Briefly, 5 mg of the dried extract was transferred separately into clean, dry and stoppered glass tubes and 1 mL of each solvent was added to obtain a nominal extract concentration of 5 mg mL^{-1}. Each mixture was vortexed for 1 min using the BenchMixer BV1000 vortex mixer and subsequently sonicated for 10 min in the Elmasonic S 30 H ultrasonic bath at room temperature (25 ± 2°C). The tubes were allowed to stand undisturbed for 30 min and were then visually examined against white and black backgrounds for solution clarity, turbidity, sediment formation and visible undissolved particles. The extract was classified as soluble when a clear, homogeneous solution without visible particles or sediment was obtained and as insoluble when persistent undissolved material remained after vortexing, sonication and standing. Each determination was performed independently in triplicate. The selection of solvents was based on recent reports describing the hydrophobic behaviour of curcuminoids and their preferential dissolution or extraction in organic solvents compared with water (Slacek *et al*., 2023; Moulick *et al*., 2025).

In-silico analysis

Ligand selection and preparation

Active compounds identified in the CL extract, specifically curcumin and its derivatives, demethoxycurcumin and bisdemethoxycurcumin, were selected for the *in-silico* docking study. These compounds were identified using HPLC. The canonical Simplified Molecular Input Line Entry System (SMILES) strings and three-dimensional structures of curcumin, demethoxycurcumin and bisdemethoxycurcumin were obtained from PubChem (National Center for Biotechnology Information, 2026; Fig. 2). The structures were downloaded and converted into Protein Data Bank, partial charge (Q) and atom type (T) (PDBQT) format using Open Babel in PyRx 0.8. The PDBQT files were subsequently used for molecular docking simulations (Eberhardt *et al*., 2021).

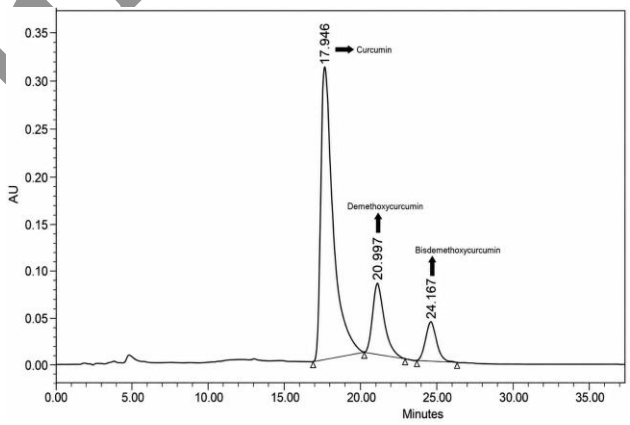


Fig. 2: Presence of curcumin, demothoxycuramin and bismethoxycircumin.

Target protein selection and preparation

Breast cancer-related proteins involved in tumor progression and apoptosis, including BCL2 (Protein Data Bank [PDB] ID: 4LVT), caspase-3 (PDB ID: 1PAU), estrogen receptor alpha (ERα; PDB ID: 3ERT), epidermal growth factor receptor (EGFR) tyrosine kinase (PDB ID: 1M17) and TOP2A (PDB ID: 1ZXM), were selected as target proteins. These proteins are involved in cancer cell proliferation, apoptosis and metastasis. The protein structures were retrieved from the Research Collaboratory for Structural Bioinformatics Protein Data Bank (RCSB PDB) (RCSB PDB, 2026). Using AutoDock Tools, water molecules were removed and Gasteiger charges were added to the protein structures. Hydrogen atoms were

Article in Press

subsequently added and the proteins were further processed to obtain appropriate conformations for molecular docking simulations (Eberhardt *et al*.,).

Molecular docking

Molecular docking simulations were performed using PyRx 0.8, which incorporates AutoDock Vina for ligand-protein interaction prediction. Grid boxes were centered on the active sites of the selected target proteins based on experimentally characterized or literature-reported binding sites. The grid dimensions were defined to encompass the relevant binding regions of each protein. Docking was performed using default settings, with ligands treated as flexible and proteins as rigid during the simulations. Binding affinities were recorded in kcal/mol and used to compare ligand-protein interactions. Docking poses were analyzed and visualized using Discovery Studio Visualizer and PyMOL. Ligand-protein interactions were evaluated based on hydrogen bonds, hydrophobic interactions and other non-covalent interactions (Eberhardt *et al*., 2021).

Absorption, distribution, metabolism, excretion and toxicity study and drug-likeness evaluation

The SMILES strings of the ligands were submitted to SwissADME and pkCSM for computational profiling. Physicochemical properties, including molecular weight, lipophilicity, water solubility, topological polar surface area, pharmacokinetic characteristics, drug-likeness and bioavailability-related parameters, were predicted using the SwissADME web tool (Daina *et al*., 2017; Swiss Institute of Bioinformatics, 2026). ADMET properties, including gastrointestinal absorption, blood-brain barrier permeability, cytochrome P450 inhibition and hepatotoxicity, were predicted using pkCSM (Pires *et al*., 2015). The compounds were also evaluated according to Lipinski's Rule of Five to assess their drug-likeness and potential for oral bioavailability.

Target prediction using SwissTargetPrediction

To investigate the broader pharmacological profiles of the identified compounds, the SMILES strings of curcumin, demethoxycurcumin and bisdemethoxycurcumin were submitted to SwissTargetPrediction. Potential human protein targets were predicted based on ligand similarity and pharmacophore features (Daina *et al*., 2019; Swiss Institute of Bioinformatics, 2026b). Docking scores were used to compare the binding affinities of the compounds toward the selected target proteins. The highest-affinity docking poses were analyzed to identify key amino acid residues involved in ligand-protein interactions. These interactions were visualized using PyMOL and Discovery Studio Visualizer and assessed for hydrogen bonds, hydrophobic interactions and other relevant non-covalent interactions. Binding affinities were reported in kcal/mol and compared across compounds to identify ligands with stronger predicted interactions with the selected proteins. Protein-ligand interaction maps were generated and the docking conformations of the ligands within the protein-binding sites were examined to assess the predicted binding modes of the ligand-protein complexes (Eberhardt *et al*., 2021).

HPLC

A 50 mg aliquot of the dried extract was mixed with 24 mL methanol, followed by the addition of 16 mL distilled water and 10 mL of 6 M hydrochloric acid. The mixture was incubated at 95°C in a thermostatically controlled water bath, cooled to room temperature and filtered through a 0.45 µm nylon membrane filter (Millipore, USA) before HPLC analysis. Chromatographic separation was performed using a Shimadzu LC-10A system equipped with a Shim-pack CLC-ODS C18 column (250 mm × 4.6 mm, 5 µm). Mobile phase A consisted of water and acetic acid (94:6, v/v; pH 2.27), whereas mobile phase B consisted of acetonitrile. The proportion of mobile phase B was increased from 15% initially to 45% at 15 min and to 100% between 35- and 45-min. Phenolic compounds were detected at 280 nm using an ultraviolet-visible detector. Compounds were identified by comparing their retention times and ultraviolet spectra with those of reference standards (Kafeel *et al*., 2023).

FT-IR

The functional-group profile of the dried CL extract was assessed using attenuated total reflectance (ATR) FT-IR spectroscopy. Approximately 2 mg of dried extract was placed directly onto the diamond ATR crystal of the Nicolet iS5 FT-IR spectrometer. Spectra were recorded over the range of 4000–400 cm^{-1} at a resolution of 4 cm^{-1} with 32 scans per sample. A background spectrum was collected before each run and automatically subtracted. Characteristic peaks corresponding to phenolic hydroxyl, conjugated carbonyl, aromatic carbon-carbon stretching and ether functional groups were interpreted using standard infrared spectral interpretation methods (Silverstein *et al*., 2014).

LC-MS

LC-MS analysis was performed to confirm the major curcuminoids present in the CL extract. A 50 mg aliquot of dried extract was dissolved in 24 mL HPLC-grade methanol, followed by the addition of 16 mL distilled water and 10 mL of 6 M hydrochloric acid. The mixture was incubated at 95°C for 2 h, cooled to room temperature and filtered through a 0.45 µm nylon syringe filter. The final volume was adjusted to 100 mL with methanol before analysis. Chromatographic separation was performed using the Shimadzu LC-10A system with a Shim-pack CLC-ODS C18 column (250 mm × 4.6 mm, 5 µm). The mobile phases and gradient programme were the same as those described for HPLC. The column effluent was introduced into the QTRAP 4500 tandem mass spectrometry system equipped with an electrospray ionisation source operating in positive-ion mode. The ion spray voltage was 5.5 kV, curtain gas was 35 psi, nebuliser

Article in Press

gas was 50 psi, turbo gas was 50 psi and source temperature was 550°C. Full-scan spectra were acquired over a mass-to-charge ratio (m/z) range of 100–800. Data-dependent tandem mass spectrometry fragmentation was performed for the three most intense ions per scan using nitrogen as the collision gas and a collision energy of 35 eV. Curcuminoids were identified by comparing retention times, m/z values and fragmentation patterns with authentic standards and published curcuminoid mass spectral data.

Cell line source, authentication and culture conditions

MDA-MB-231 breast cancer cells and MCF-10A non-tumorigenic mammary epithelial cells were obtained from the Centre of Excellence in Molecular Biology (CEMB), University of the Punjab, Lahore, Pakistan. The cell lines corresponded to the American Type Culture Collection (ATCC) reference lines MDA-MB-231 (ATCC® HTB-26™) and MCF-10A (ATCC® CRL-10317™). MDA-MB-231 cells were used at passage 3, whereas MCF-10A cells were used at passage 4. The identity of each cell line was evaluated against the short tandem repeat (STR) profiles reported by ATCC and Cellosaurus. The published reference STR allele profiles for MDA-MB-231 and MCF-10A are provided in table S1. These reference profiles were used to confirm the expected identity markers of the respective cell lines. Cells were routinely examined for characteristic adherent morphology and evidence of contamination and cultures showing abnormal morphology or microbial contamination were discarded. MDA-MB-231 cells were maintained in DMEM supplemented with 10% FBS and 1% penicillin-streptomycin. MCF-10A cells were maintained in DMEM/F-12 medium supplemented with 5% horse serum, 20 ng mL^{-1} epidermal growth factor, 10 µg mL^{-1} insulin, 0.5 µg mL^{-1} hydrocortisone, 100 ng mL^{-1} cholera toxin and 1% penicillin-streptomycin. Both cell lines were cultured at 37°C in a humidified incubator containing 5% carbon dioxide. All cell culture procedures were performed under aseptic conditions in a Class II biosafety cabinet. Culture morphology and confluence were monitored using an inverted microscope. Cell culture handling followed standard mammalian cell culture procedures (Freshney, 2010).

Subculturing and cell counting

When cells reached approximately 80–90% confluence, the culture medium was removed and the cells were washed with sterile PBS. Trypsin-EDTA solution was added to detach the cells and the flasks were incubated briefly at 37°C until detachment occurred. Complete medium was then added to neutralise trypsin activity and the cells were gently resuspended by pipetting. Cells were centrifuged at 300 × g for 5 min at room temperature when pelleting was required. Viable cells were counted using the CellDrop FL automated cell counter. Cell viability during routine culture was also assessed by trypan blue exclusion when required (Strober, 2015).

MTT cell viability assay

Cell viability was assessed using the MTT assay with minor modifications. MDA-MB-231 and MCF-10A cells were seeded in 96-well plates at a density of 1×10^4 cells per well in 100 µL complete medium and allowed to adhere for 24 h at 37°C in 5% carbon dioxide. Cells were then treated with CL extract or DOX at concentrations of 8, 16, 32, 64, 128 and 256 µg mL^{-1} for 24 h (Table 1). Vehicle-treated wells were included as controls and blank wells containing medium without cells were also included (Arshad and Afridi, 2025). After treatment, 50 µL of MTT solution at 5 mg mL^{-1} in PBS was added to each well and the plates were incubated for 2 h at 37°C in the dark. The medium was carefully removed and 100 µL DMSO was added to each well to dissolve the formazan crystals. The plates were shaken for 15 min at room temperature to ensure complete dissolution. Absorbance was measured at 570 nm using the RT-6000 microplate reader. Cell viability was calculated as a percentage of vehicle control. IC_{50} values were calculated by nonlinear regression using GraphPad Prism version 8.0.1 (GraphPad Software, San Diego, CA, USA).

Table 1: Two-fold prepared dose concentrations of *Curcuma longa* extract.

Number of concentrations	Dose concentration (µg mL^{-1})
1st	256
2nd	128
3rd	64
4th	32
5th	16
6th	8

Trypan blue exclusion assay

The trypan blue exclusion assay was used to determine viable and non-viable cell counts, as described previously (Strober, 2015). MDA-MB-231 and MCF-10A cells were seeded in six-well plates at 5×10^5 cells per well and incubated for 24 h. The medium was replaced with fresh medium containing CL extract or DOX at 20, 40 or 80 µg mL^{-1}. Control wells received the corresponding vehicle. After 24 h of treatment, both floating and adherent cells were collected. Adherent cells were detached using trypsin-EDTA solution, pooled with the floating cells and centrifuged at 300 × g for 5 min at room temperature. The cell pellet was resuspended in fresh medium and mixed with trypan blue solution in a 1:1 ratio. Viable and dead cells were counted using the CellDrop FL automated cell counter. Results were expressed as the percentage of viable cells relative to the control group.

Phase-contrast morphological assessment

Morphological changes associated with cytotoxicity and apoptosis were evaluated by phase-contrast microscopy. MDA-MB-231 cells were seeded in 24-well plates at 1×10^5 cells per well and incubated overnight. Cells were

Article in Press

treated with CL extract at 20, 40 and 80 µg mL^{-1} for 24 h. Untreated and vehicle-treated cells served as controls. Morphological features, including cell shrinkage, rounding, detachment and membrane blebbing, were observed using an inverted phase-contrast microscope at 100× magnification. Representative images were captured using the microscope imaging system (Arshad and Saleem, 2025).

Annexin V/PI apoptosis staining

Apoptotic changes were assessed using an Annexin V-FITC/PI Apoptosis Detection Kit, following the manufacturer's protocol and the principle described by Vermes *et al*. (1995). MDA-MB-231 cells were seeded in six-well plates at 5 × 10^5 cells per well and incubated overnight. Cells were treated with CL extract at 20, 40 and 80 µg mL-¹ for 24 h. After treatment, both floating and adherent cells were collected, washed twice with cold PBS and resuspended in binding buffer. Annexin V-FITC (5 µL) was added and the cells were incubated for 10 min in the dark. PI (10 µL) was then added and the cells were examined immediately using a fluorescence-equipped inverted microscope at 100× magnification. Green fluorescence indicated early apoptotic cells, whereas red fluorescence indicated late apoptotic or necrotic cells.

Hoechst 33342/PI nuclear staining

Nuclear morphological changes were evaluated using Hoechst 33342 and PI double staining, adapted from fluorescence-based apoptosis assessment methods (Ribble *et al*., 2005; Krysko *et al*., 2008). MDA-MB-231 cells were seeded in 24-well plates at 1 × 10^5 cells per well and incubated overnight. Cells were treated with CL extract at 20, 40 and 80 µg mL-¹ for 24 h. After treatment, the cells were washed with PBS and stained with Hoechst 33342 at 10 µg mL-¹ for 10 min at 37°C in the dark. PI was then added at 2.5 µg mL-¹ for 5 min at room temperature in the dark. Stained cells were visualised using the fluorescence-equipped inverted microscope at 200× magnification. Condensed or fragmented blue nuclei were interpreted as apoptotic nuclei, whereas red-stained nuclei indicated loss of membrane integrity (Arshad and Afridi, 2025).

ROS assay

Intracellular ROS generation was measured using the DCFH-DA assay, adapted from published dichlorofluorescein-based ROS measurement methods (Wang and Joseph, 1999; Eruslanov and Kusmartsev, 2010). MDA-MB-231 and MCF-10A cells were seeded in black, clear-bottom 96-well plates at 1 × 10^5 cells per well in 100 µL complete medium and incubated overnight. Cells were treated with CL extract or DOX at 20, 40 and 80 µg mL^{-1} for 24 h. Vehicle-treated cells and blank wells were included. After treatment, the medium was removed and the cells were washed with PBS. Freshly prepared DCFH-DA working solution at 10 µM was added to each well at 100 µL. The plates were incubated at 37°C for 1 h in the dark. Fluorescence was measured at an excitation wavelength of 485 nm and an emission wavelength of 535 nm using the Varioskan ALF multimode microplate reader. Background fluorescence from blank wells was subtracted. ROS production was expressed as fold change relative to the matched vehicle control (Arshad and Saleem, 2025).

Scratch wound-healing assay

Cell migration was evaluated using the scratch wound-healing assay described by Liang *et al*. (2007), with minor modifications. MDA-MB-231 cells were seeded in six-well plates at 1.75 × 10^5 cells mL-¹ in 2 mL complete medium and cultured until a confluent monolayer was formed. A straight scratch was made in each well using a sterile 200 µL pipette tip. Detached cells were removed by washing twice with PBS. Cells were then incubated in low-serum medium containing 1% serum and treated with CL extract at the IC_{50} concentration. Control wells received vehicle only. Images of the scratch area were captured at 0, 24, 48 and 72 h using the inverted microscope. Wound area was quantified using ImageJ software version 1.54t. Wound closure was calculated using the following formula:

Wound closure (%) = $[(A_0 - A_i) / A_0] \times 100$

where A_0 is the wound area at 0 h and A_i is the wound area at each subsequent time point.

LDH cytotoxicity assay

Membrane damage was assessed by measuring LDH release according to the principle described by Decker and Lohmann-Matthes (1988). MDA-MB-231 and MCF-10A cells were seeded in black, clear-bottom 96-well plates at 1 × 10^4 cells per well and allowed to adhere for 24 h. Cells were treated with CL extract or DOX at 20, 40 and 80 µg mL-¹ for 24 h. Vehicle-treated wells were used as negative controls. Maximum-release control wells were treated with 0.1% Triton X-100 during the final 30 min of exposure. After treatment, 100 µL of cell-free supernatant from each well was transferred to a new black 96-well plate. An equal volume of CytoTox-ONE™ LDH release reagent was added and the mixture was incubated for 10 min at room temperature in the dark. Stop solution (50 µL) was then added. Fluorescence was recorded at an excitation wavelength of 560 nm and an emission wavelength of 590 nm using the Infinite M1000 Pro microplate reader. Blank signals were subtracted from all readings. LDH release was expressed as raw fluorescence units and percentage cytotoxicity relative to the maximum-release controls.

Mitochondrial membrane potential assay

ΔΨm was measured using JC-1 staining. MDA-MB-231 and MCF-10A cells were seeded and allowed to adhere overnight. Cells were treated with CL extract or DOX at 20, 40 and 80 µg mL-¹ for 24 h. Vehicle-treated wells were included for each treatment. After treatment, both floating

Article in Press

and adherent cells were collected, washed with warm PBS and resuspended in pre-warmed Hanks' balanced salt solution (HBSS) at approximately 1×10^6 cells mL^{-1}.
Freshly prepared JC-1 working solution was added at a final concentration of 2 µM and the cells were incubated for 20 min at 37°C in the dark. Cells were then centrifuged at 300 × g for 5 min, washed once with warm HBSS and resuspended at $0.5–1 \times 10^6$ cells mL^{-1}. Samples were analysed immediately using the CellDrop FL automated cell counter with green and red fluorescence channels enabled. The depolarisation control consisted of cells treated with CCCP at 10 µM for 20 min before staining. Unstained cells, single-stain controls and drug-only controls were included to assess background fluorescence and autofluorescence. The ΔΨm index was calculated as the red-to-green fluorescence ratio and normalised to the matched vehicle control (Arshad and Afridi, 2025).

Caspase-3/7 and caspase-9 activity assays
Caspase activity was measured using colorimetric assay kits based on cleavage of peptide p-nitroanilide substrates and on published caspase substrate methods (Thornberry *et al*., 1997). Caspase-3/7 activity was assessed using the Caspase 3 Assay Kit, Colorimetric, whereas caspase-9 activity was assessed using the Caspase-9 Colorimetric Activity Assay Kit. MDA-MB-231 and MCF-10A cells were seeded in six-well plates at 2×10^5 cells per well and allowed to adhere overnight. Cells were treated with CL extract or DOX at 20, 40 and 80 µg mL^{-1} for 24 h. Vehicle-treated wells were included as controls.

After treatment, floating and adherent cells were collected and washed with ice-cold PBS. Cells were lysed on ice in kit lysis buffer for 10 min and centrifuged at 10,000 × g for 10 min at 4°C. Supernatants were collected as cytosolic extracts. Protein concentration was measured using the BCA assay. Equal amounts of protein were used for all reactions. For caspase-3/7 activity, 100 µg of protein was incubated in reaction buffer containing 10 mM dithiothreitol and the DEVD-p-nitroanilide substrate. For caspase-9 activity, the same protocol was used with LEHD-p-nitroanilide substrate. Substrate blanks and vehicle controls were included. Specificity controls were prepared by pre-incubating lysates with Ac-DEVD-CHO or Ac-LEHD-CHO inhibitors for 15 min on ice before substrate addition. Plates were incubated for 1–2 h at 37°C and absorbance was measured at 405 nm using the Infinite M1000 Pro microplate reader. Activities were expressed as absorbance change normalised to protein content and subsequently normalised to the matched vehicle control (Arshad and Afridi, 2025).

RT-qPCR
RT-qPCR was performed to assess the expression of apoptosis- and proliferation-related genes. MDA-MB-231 and MCF-10A cells were seeded in six-well plates at 2×10^5 cells per well and allowed to adhere overnight. Cells were treated with CL extract or DOX at 20, 40 and 80 µg mL^{-1} for 24 h. Total RNA was extracted using TRIzol™ Reagent according to the manufacturer's protocol. RNA concentration and purity were assessed by measuring absorbance at 260 and 280 nm using the NanoDrop One spectrophotometer. RNA samples were treated with DNase I to remove genomic DNA contamination. cDNA was synthesised from 1 µg total RNA using the iScript™ cDNA Synthesis Kit in a 20 µL reaction. RT-qPCR was performed using the CFX96 detection system. Each 20 µL reaction contained 10 µL SsoAdvanced™ Universal SYBR® Green Supermix, 0.4 µL forward primer, 0.4 µL reverse primer, 2 µL diluted cDNA and 7.2 µL nuclease-free water. The target genes were *BAX*, *BCL2*, *CASP9* and *TOP2A*. Glyceraldehyde-3-phosphate dehydrogenase (*GAPDH*) was used as the reference gene. Primer sequences are shown in table 2.

The thermal cycling conditions were 95°C for 3 min, followed by 40 cycles of 95°C for 10 s and 60°C for 30 s. Melt-curve analysis was performed from 65°C to 95°C to confirm amplification specificity. No-template and no-reverse-transcription controls were included in each run. Relative gene expression was calculated using the $2^{-}\Delta\Delta Cq$ method (Livak and Schmittgen, 2001). Technical duplicates differing by more than 0.5 Cq were repeated.

Statistical analysis
Data were analysed using GraphPad Prism version 8.0.1 (GraphPad Software, San Diego, CA, USA). Quantitative results were expressed as mean ± standard deviation (SD). Dose-response curves were generated using a four-parameter logistic regression model and IC_{50} values were reported with 95% confidence intervals (CIs). Dose effects within each treatment group were analysed by one-way analysis of variance (ANOVA) followed by Dunnett's multiple-comparison test when the assumptions were met. Comparisons between CL and DOX at matched concentrations were performed using two-way ANOVA followed by Sidak's multiple-comparison test. Comparisons between MDA-MB-231 and MCF-10A cells were performed using Welch's t-test when appropriate. Normality was assessed using the Shapiro-Wilk test and homogeneity of variance was assessed using the Brown-Forsythe test. When the assumptions were violated, the Kruskal-Wallis test, followed by Dunn's post hoc test, was applied. Multiple comparisons were controlled using the Benjamini-Hochberg false discovery rate method. A p-value <0.05 was considered statistically significant.

RESULTS

Solubility of the Curcuma longa extract
The dried DCM extract of CL was soluble in chloroform, acetone, ethanol and methanol but remained insoluble in

Article in press

distilled water under the experimental conditions described above. The qualitative solubility findings are presented in table 3.

Table 2: Primer sequences used for RT-qPCR analysis of apoptosis and proliferation markers.

Target gene	Forward primer (5′→3′)	Reverse primer (5′→3′)
BAX	TTTGCTTCAGGGTTTCATCC	TTCAGCTTCTTGGTGGATGA
BCL2	TGTGGATGACTGAGTACCTGAACC	GGGCCGTACAGTTCCACAAA
CASP9	TGGAGCAGCTTCTGTTTCCT	CAGGACAAAGCCTCCATCTC
TOP2A	GAGGAGCTGTTGGAGATGCT	TCTCTGGCTTCTTGCTCTGG

Table 3: Qualitative solubility of the dried dichloromethane extract of *Curcuma longa* in different solvents

Solvent	Solubility observation
Distilled water	Insoluble
Chloroform	Soluble
Acetone	Soluble
Ethanol	Soluble
Methanol	Soluble

In-silico results

The canonical SMILES strings and three-dimensional structures of curcumin, demethoxycurcumin and bisdemethoxycurcumin were retrieved from PubChem and converted into PDBQT format using Open Babel in PyRx 0.8.

The molecular weight, polar surface area (PSA) and logP values of the three compounds were calculated as follows:

- ***Curcumin***: molecular weight = 368.38 g mol-¹, logP = 3.3, PSA = 106.56 Å²
- ***Demethoxycurcumin***: molecular weight = 338.36 g mol-¹, logP = 3.2, PSA = 108.45 Å²
- ***Bisdemethoxycurcumin***: molecular weight = 308.35 g mol-¹, logP = 3.1, PSA = 109.23 Å²

These physicochemical properties indicate moderate lipophilicity and are consistent with drug-like characteristics.

Protein preparation and docking

Docking simulations were conducted using five breast cancer-related target proteins: BCL2, caspase-3, ERα, EGFR and TOP2A. The binding affinities of each ligand-protein complex were calculated and expressed as binding energies in kcal mol-¹. The results are presented in table 4. The results showed that curcumin exhibited the strongest predicted binding affinity among the tested compounds, particularly toward BCL2 and ERα, suggesting favorable interactions with these targets.

Docking analysis indicated that curcumin interacted with key amino acid residues of the target proteins through hydrogen bonds and hydrophobic interactions:

- ***BCL2***: Hydrogen bonds were observed with TYR67, ARG66 and GLY104, together with hydrophobic interactions within the binding pocket.
- ***ERα***: Binding interactions involved SER305 and MET365.
- ***EGFR***: Curcumin interacted with residues within the adenosine triphosphate (ATP)-binding site, particularly LYS721 and ASP831.

ADMET profiling and drug-likeness

ADMET predictions obtained with SwissADME and pkCSM were used to evaluate the pharmacokinetic profiles of the compounds. The main findings were as follows:

- ***Gastrointestinal (GI) absorption***: All three compounds showed moderate to high predicted GI absorption, with values of 89% for curcumin, 87% for demethoxycurcumin and 85% for bisdemethoxycurcumin.
- ***Blood-brain barrier (BBB) permeability***: All three compounds showed low predicted BBB permeability, with values of 0.12 for curcumin, 0.09 for demethoxycurcumin and 0.07 for bisdemethoxycurcumin.
- ***Lipinski's Rule of Five***: All three compounds complied with Lipinski's Rule of Five, indicating physicochemical characteristics compatible with oral drug-likeness.
- ***Cytochrome P450 3A4 (CYP3A4) inhibition***: Curcumin showed moderate predicted inhibition of CYP3A4, whereas demethoxycurcumin and bisdemethoxycurcumin showed negligible predicted inhibition.

Target prediction

SwissTargetPrediction suggested that curcumin, demethoxycurcumin and bisdemethoxycurcumin may interact with several human proteins involved in cancer-related signaling pathways. Notable predicted targets included:

- ***Curcumin***: Predicted targets included phosphoinositide 3-kinase (PI3K), mitogen-activated protein kinases (MAPKs), protein kinase B (AKT) and BCL2, which are involved in cell survival, proliferation and apoptosis.
- ***Demethoxycurcumin and bisdemethoxycurcumin***: Predicted targets included cyclin-dependent kinase 2 (CDK2), tumor protein p53 (TP53), BCL2, EGFR and other proteins associated with cell signaling and apoptosis.

Molecular visualization

Protein-ligand interactions were visualized using Discovery Studio Visualizer and PyMOL. The interaction maps showed hydrophobic interactions and hydrogen

Article in Press

bonds between curcumin and the selected target proteins. These interactions were particularly evident for BCL2 and ERα and supported the predicted docking affinities of curcumin toward these proteins.

Table 3: Binding affinities for each ligand-protein complex.

Protein	Curcumin (kcal/mol)	Demethoxycurcumin (kcal/mol)	Bisdemethoxycurcumin (kcal/mol)
Bcl-2	-9.2	-8.4	-8.1
Caspase-3	-8.7	-7.9	-7.6
Estrogen Receptor α	-9.0	-8.3	-8.0
EGFR	-8.5	-7.8	-7.5
Topoisomerase IIα	-8.8	-8.1	-7.9

Table 4: Summary of *in-silico* profiling for curcumin and two curcumin derivatives.

Protein	Curcumin (kcal/mol)	Demethoxycurcumin (kcal/mol)	Bisdemethoxycurcumin (kcal/mol)
Bcl-2	-9.2	-8.4	-8.1
Caspase-3	-8.7	-7.9	-7.6
Estrogen receptor α	-9.0	-8.3	-8.0
EGFR	-8.5	-7.8	-7.5
Topoisomerase IIα	-8.8	-8.1	-7.9
Gastrointestinal absorption (%)	89%	87%	85%
Blood-brain barrier (LogBB)	0.12	0.09	0.07
Lipinski's rule of five compliance	Yes	Yes	Yes
CYP3A4 inhibition	Moderate	Low	Negligible
Swiss Target Prediction Results for Curcuma longa Compounds			
Curcumin	PI3K, MAPKs, AKT, Bcl-2, CDK2, TP53		
Demethoxycurcumin	CDK2, TP53, Bcl-2, p53, EGFR, HSP90 (heat shock protein)		
Bisdemethoxycurcumin	PI3K, CDK2, TP53, HSP90, Bcl-2, EGFR		
Molecular Interactions in Protein-Ligand Docking			
Bcl-2	Hydrogen bonds with TYR67, ARG66, GLY104; hydrophobic interactions		
Caspase-3	Hydrophobic interactions with PHE-106, ILE-106		
Estrogen receptor α	Hydrogen bonds with SER305, MET365		
EGFR	Hydrogen bonds with LYS721, ASP831		
Topoisomerase IIα	Hydrophobic interactions with ILE406, TYR529 and hydrophilic interactions		

Overall docking and drug-likeness results

Based on the predicted binding affinities and ADMET profiles, curcumin showed the most favorable overall *in-silico* profile among the three compounds and was therefore identified as the leading candidate for further experimental validation (Table 5). Demethoxycurcumin and bisdemethoxycurcumin also showed predicted interactions with the selected target proteins, although their binding affinities were generally weaker than those of curcumin. These findings support further experimental investigation of the three curcuminoids, particularly curcumin, rather than direct conclusions regarding their clinical efficacy.

HPLC results

HPLC analysis identified curcumin, demethoxycurcumin and bisdemethoxycurcumin as the major curcuminoids present in the CL extract, as shown in figure 2.

FT-IR spectroscopy results

The ATR-FT-IR spectrum of the CL extract showed characteristic absorbance bands consistent with phenolic hydroxyl, conjugated diketone and aromatic functional groups associated with curcuminoids. A broad O–H stretching vibration was observed at 3435 cm^{-1}, indicating hydrogen-bonded phenolic groups. Weak C–H stretching vibrations of aliphatic groups were observed at 2925 and 2854 cm^{-1}. A prominent conjugated C=O stretching band appeared at 1627 cm^{-1}, while aromatic C=C stretching vibrations were observed at 1601 and 1508 cm^{-1}. A strong C–O stretching band corresponding to phenolic ether groups was detected at 1276 cm^{-1} and aromatic C–H out-of-plane bending vibrations were observed at 963 and 817 cm^{-1}. These spectral features were consistent with the expected FT-IR profiles of curcumin, demethoxycurcumin and bisdemethoxycurcumin (Table 6) and supported the presence of curcuminoid-related functional groups in the DCM extract.

LC-MS results for CL extract

LC-MS analysis revealed three major curcuminoid peaks corresponding to:

Article in Press

1. ***Curcumin***: m/z = 369.13 $[M+H]^+$; retention time (tR) ≈ 33 min
2. ***Demethoxycurcumin***: m/z = 339.11 $[M+H]^+$; tR ≈ 30 min
3. ***Bisdemethoxycurcumin***: m/z = 309.10 $[M+H]^+$; tR ≈ 27 min

Table 6: FT-IR band assignments for the *Curcuma longa* DCM extract.

Wavenumber (cm^{-1})	Assignment
3435	O–H stretching (phenolic hydroxyl)
2925, 2854	C–H stretching (aliphatic methylene groups)
1627	C=O stretching (conjugated diketone in curcuminoids)
1601, 1508	C=C stretching (aromatic ring)
1276	C–O stretching (phenolic ether linkage)
1024	C–O–C stretching (aryl–ether)
963, 817	Aromatic C–H out-of-plane bending

Table 7: Each cell line/treatment to test for dose effects. The results were expressed as the mean±SD (n= 3).

Dose (µg/mL)	DOX Mean ± SD (% viability)	DOX Sig.	CL Mean ± SD (% viability)	CL Sig.	CL Mean ± SD (% viability)	CL Sig.	DOX Mean ± SD (% viability)	DOX Sig.
	For MDA-MB-231 cells				For MCF-10A cells			
8	80.7 ± 0.9	***	84.4 ± 3.0	**	99.4 ± 1.0	ns	89.9 ± 2.2	*
16	62.7 ± 2.0	***	63.9 ± 1.5	***	99.3 ± 0.7	ns	85.7 ± 0.7	***
32	41.3 ± 2.1	***	43.9 ± 1.3	***	97.4 ± 0.5	*	66.7 ± 1.5	***
64	22.8 ± 0.9	***	26.8 ± 0.8	***	98.3 ± 1.4	ns	44.9 ± 1.9	***
128	10.6 ± 1.4	***	15.5 ± 1.5	***	97.4 ± 0.6	*	27.5 ± 1.8	***
256	5.7 ± 0.6	***	7.6 ± 0.9	***	96.4 ± 1.1	ns	14.8 ± 0.8	***
	Doxorubicin		CL extract		CL extract		Doxorubicin	
IC_{50} (µg·mL^{-1})	23.62		18.50		>256		52.36	

Where "ns" = not significant at α=0.05; * p<0.05; ** p<0.01; *** p<0.001.

These assignments were supported by comparison of retention times and tandem mass spectrometry (MS/MS) fragmentation patterns with authentic standards. Based on ultraviolet (UV) peak areas at 280 nm and mass spectrometric signal intensities, curcumin accounted for approximately 45–50% of the total curcuminoid content, demethoxycurcumin for approximately 25–30% and bisdemethoxycurcumin for approximately 20–25%.

Minor peaks, each representing <5% of the total peak area, were observed at earlier retention times of approximately 15–20 min. These peaks were consistent with other diarylheptanoid- or sesquiterpene-related constituents but were not further characterised in the present study. The three principal curcuminoids showed characteristic UV absorbance maxima near 420 nm and distinct MS/MS fragmentation patterns. Curcumin produced major fragment ions at m/z 177.09 and 219.10, demethoxycurcumin at m/z 149.06 and 177.09 and bisdemethoxycurcumin at m/z 137.05 and 177.09. The HPLC chromatogram in figure 2 shows the peaks corresponding to curcumin, demethoxycurcumin and bisdemethoxycurcumin, which were further supported by LC-MS analysis.

MTT results

Both CL extract and DOX produced a marked dose-dependent reduction in MDA-MB-231 cell viability (ANOVA, $p < 5 \times 10^{-15}$). In MCF-10A cells, CL extract produced only small changes in viability of ≤3.6%, with no statistically significant overall dose effect (Kruskal-Wallis test, p = 0.053). In contrast, DOX produced significant dose-dependent cytotoxicity in MCF-10A cells (ANOVA, $p \approx 1.3 \times 10^{-15}$), although its effect remained greater in MDA-MB-231 cells at matched concentrations (Table 7; Fig. 3).

Four-parameter logistic regression showed comparable cytotoxic potency of CL extract and DOX against MDA-MB-231 cells, with IC_{50} values of 18.50 and 23.62 µg mL^{-1}, respectively (F-test, p = 0.056). In MCF-10A cells, the IC_{50} of CL extract remained >256 µg mL^{-1}, whereas the IC_{50} of DOX was 52.36 µg mL^{-1}. Accordingly, the selectivity index (SI), calculated as the IC_{50} in MCF-10A cells divided by that in MDA-MB-231 cells, was >13.8 for CL extract and approximately 2.22 for DOX.

Trypan blue assay results

Trypan blue exclusion showed a dose-dependent reduction in MDA-MB-231 cell viability following treatment with either CL extract or DOX across concentrations of 20–80 µg mL^{-1}. In contrast, the CL extract maintained MCF-10A viability at approximately 98–100%, whereas DOX reduced it. These findings were consistent with greater cancer-cell selectivity of the CL extract.

Morphological analysis

Phase-contrast microscopy results

Article in Press

Distinct morphological differences were observed between treated and control MDA-MB-231 cells. CL treatment produced cell shrinkage, rounding, detachment and membrane blebbing. These morphological alterations became progressively more pronounced as the CL concentration increased from 20 to 80 µg mL^{-1} compared with untreated cells (Fig. 4).

integrity. The apoptotic changes became more evident as CL concentrations increased (Fig. 5).

Hoechst 33342/PI results

Hoechst 33342/PI staining showed characteristic apoptosis-associated nuclear changes in MDA-MB-231 cells after 24 h of CL treatment. Nuclear condensation and

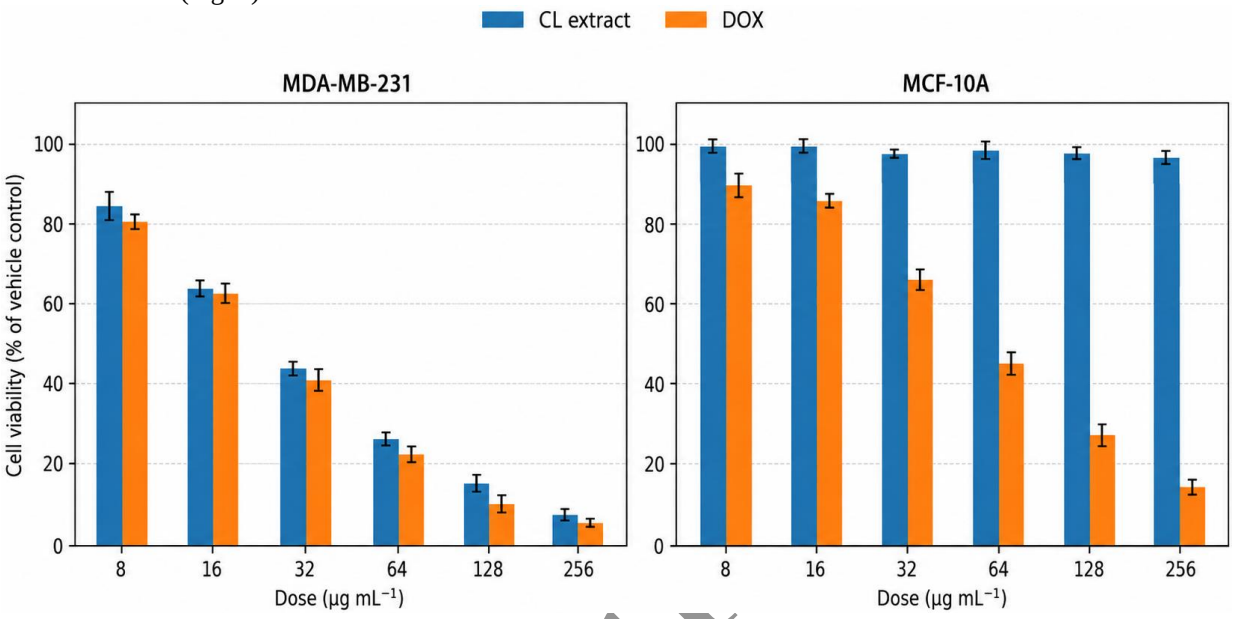


Fig. 3: Effect of CL extract and DOX on the viability of MDA-MB-231 and MCF-10A cells determined using the MTT assay. Cells were treated with CL extract or DOX at 8, 16, 32, 64, 128 and 256 µg mL^{-1} for 24 h. Cell viability was expressed as a percentage of the corresponding vehicle control. Data are presented as mean ± SD from three independent experiments (n = 3).

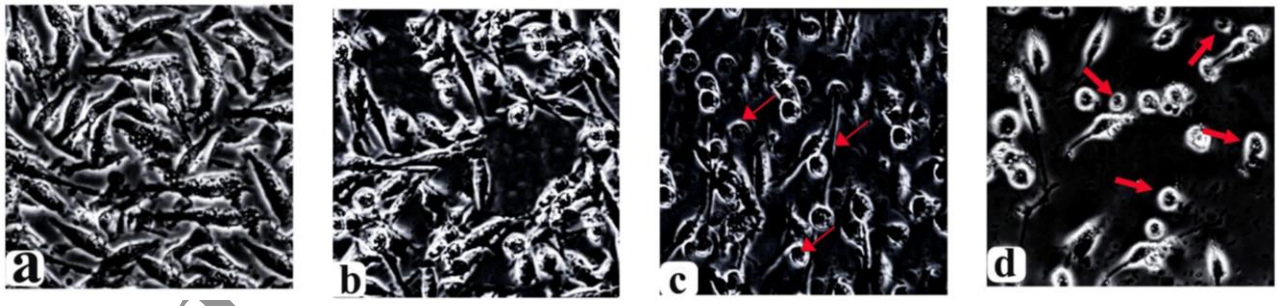


Fig. 4: Phase-contrast microscopic morphology of MDA-MB-231 cells after 24 h exposure to *Curcuma longa* extract. Panel (A) shows untreated/vehicle-control cells with normal adherent, spindle-shaped morphology. Panels (B), (C) and (D) show cells treated with 20, 40 and 80 µg mL^{-1} CL extract, respectively. Treatment caused concentration-dependent morphological changes, including reduced cell density, cell shrinkage, rounding, detachment and membrane blebbing. The red arrows indicate rounded, detached and blebbed cells, supporting CL-induced cytotoxic and apoptotic morphological alterations.

Annexin V/PI results

Annexin V/PI staining showed increased apoptotic changes in MDA-MB-231 cells following treatment with increasing concentrations of CL extract. Green fluorescence indicated Annexin V-positive early apoptotic cells, whereas increased double-positive fluorescence indicated progression toward late apoptosis or loss of membrane

fragmentation increased with increasing CL concentrations, while PI-positive nuclei indicated loss of membrane integrity and late-stage apoptotic changes. These findings supported a concentration-dependent induction of apoptotic morphological alterations by CL extract (Fig. 6).

ROS results

CL extract produced a significantly greater increase in ROS generation in MDA-MB-231 cells than in MCF-10A cells across all tested concentrations (20–80 μg mL^{-1}; $p \leq 0.0017$), indicating cancer-selective oxidative stress induction. In contrast, the difference between MDA-MB-231 and MCF-10A cells following DOX treatment was significant only at 40 and 80 μg mL^{-1} ($p \approx 0.025$) and was not significant at 20 μg mL^{-1}. These findings indicate greater selectivity of CL extract than DOX for ROS induction under the tested conditions (Fig. 7).

Article in Press

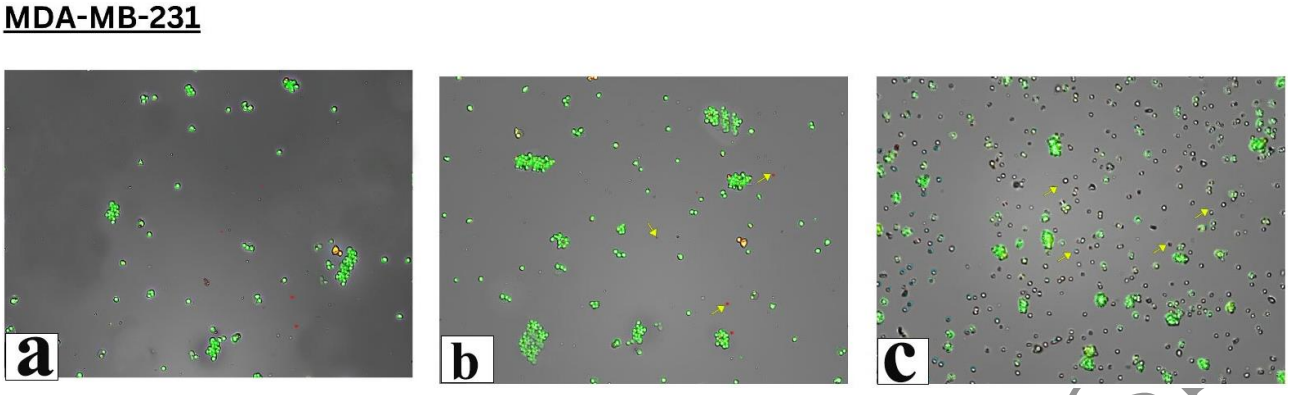


Fig. 5: Annexin V-FITC/propidium iodide fluorescence microscopy of MDA-MB-231 cells following 24 h exposure to *Curcuma longa* extract. Panels (a), (b) and (c) represent cells treated with 20, 40 and 80 µg mL^{-1} CL extract, respectively. Green fluorescence indicates Annexin V-FITC-positive apoptotic cells, whereas yellow, orange or red fluorescence indicates Annexin V/PI double-positive cells with compromised membrane integrity. The progressive increase in fluorescent cells indicates concentration-dependent induction of apoptosis. Images were captured at 100× magnification. CL, *Curcuma longa*; FITC, fluorescein isothiocyanate; PI, propidium iodide.

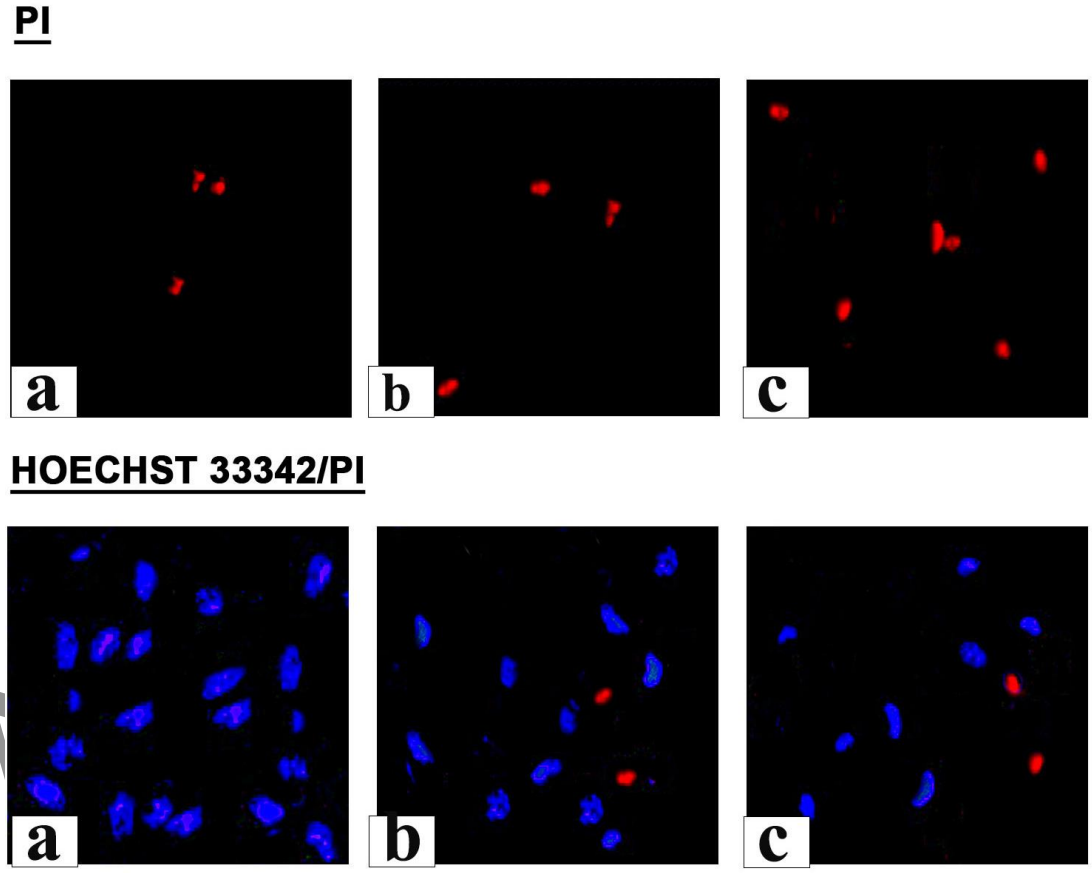


Fig. 6: Fluorescence microscopic evaluation of propidium iodide and Hoechst 33342/propidium iodide staining in MDA-MB-231 cells treated with *Curcuma longa* extract for 24 h. The upper row shows PI staining, with panels A, B and C representing treatments with 20, 40, and 80 µg mL^{-1} CL extract, respectively. The lower row shows Hoechst 33342/PI double staining, where panels (a), (b) and (c) represent treatment with 20, 40 and 80 µg mL^{-1} CL extract, respectively. Blue fluorescence indicates Hoechst-stained nuclei, whereas red fluorescence indicates PI-positive cells with loss of membrane integrity. Increased red fluorescence and nuclear condensation/fragmentation with increasing extract concentration indicate dose-dependent apoptotic and late-apoptotic changes.

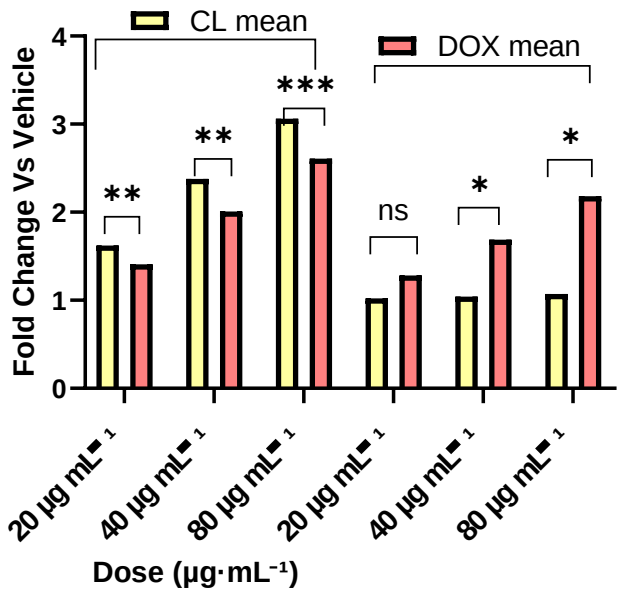


Fig. 7: Intracellular reactive oxygen species generation in MDA-MB-231 and MCF-10A cells following treatment with *Curcuma longa* extract or doxorubicin. Cells were exposed to CL extract or DOX at 20, 40 and 80 µg mL^{-1} for 24 h and DCF fluorescence was expressed as fold change relative to the matched vehicle control. Bars represent mean ± SD from three independent experiments (n=3). Statistical significance between CL and DOX at matched concentrations is indicated as ns, not significant; *p<0.05; **p<0.01; and ***p<0.001. CL, *Curcuma longa* extract; DCF, dichlorofluorescein; DOX, doxorubicin; ROS, reactive oxygen species; SD, standard deviation.

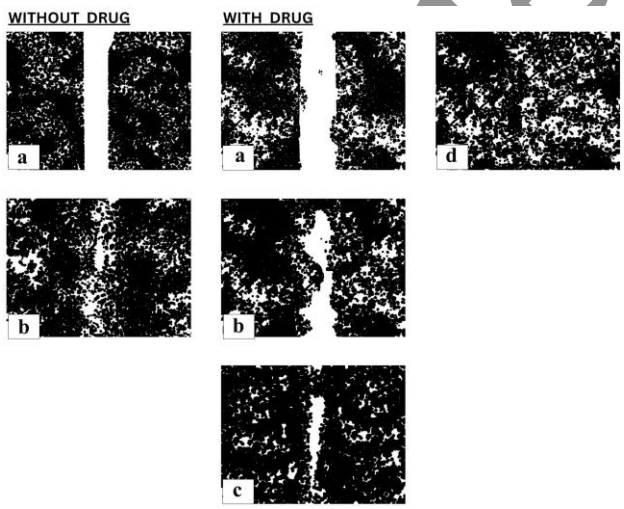


Fig. 8: Scratch wound-healing assay showing the effect of *Curcuma longa* extract on MDA-MB-231 cell migration. Panels (a) and (b) show untreated/vehicle-control cells at 0 h and 24 h, respectively. The untreated cells showed rapid wound closure, indicating active migration and proliferation. Panels (a–d) show MDA-MB-231 cells treated with *Curcuma longa* extract at the IC_{50} concentration and photographed at 0, 24, 48 and 72 h, respectively. Compared with untreated cells, CL-treated cells showed delayed wound closure, with the scratch area remaining visible for a longer period. This indicates that CL extract reduced the migratory capacity of MDA-MB-231 cells.

Wound assay results

Scratch wound-healing assay results

Untreated MDA-MB-231 cells showed complete wound closure by 24 h, whereas CL-treated cells required approximately 72 h for complete wound closure. These findings indicate that CL treatment delayed wound closure and reduced the migratory capacity of MDA-MB-231 cells under the experimental conditions (Fig. 8).

LDH results

In MDA-MB-231 cells, both CL extract and DOX produced a clear dose-dependent increase in LDH release after 24 h. The responses were similar between the two treatments at matched concentrations. Mean ± SD cytotoxicity, normalised to the 0.1% Triton X-100 maximum-release control, was 24.1 ± 3.2%, 45.8 ± 4.5% and 68.9 ± 5.4% for CL extract at 20, 40 and 80 µg mL^{-1}, respectively. The corresponding values for DOX were 26.7 ± 2.9%, 49.3 ± 3.8% and 73.5 ± 4.1%. Each condition was measured in triplicate (n = 3). In MCF-10A cells, CL extract produced only a small increase in LDH release, with cytotoxicity values of 4.3 ± 1.2%, 6.1 ± 1.5% and 8.7 ± 1.8% at 20, 40 and 80 µg mL^{-1}, respectively. In contrast, DOX produced dose-dependent increases of 12.5 ± 2.7%, 23.4 ± 3.2% and 38.9 ± 4.5% at the corresponding concentrations (n = 3 per condition). These findings show that CL extract produced cytotoxicity comparable to DOX in MDA-MB-231 cells while causing substantially less membrane damage in MCF-10A cells (Fig. 9).

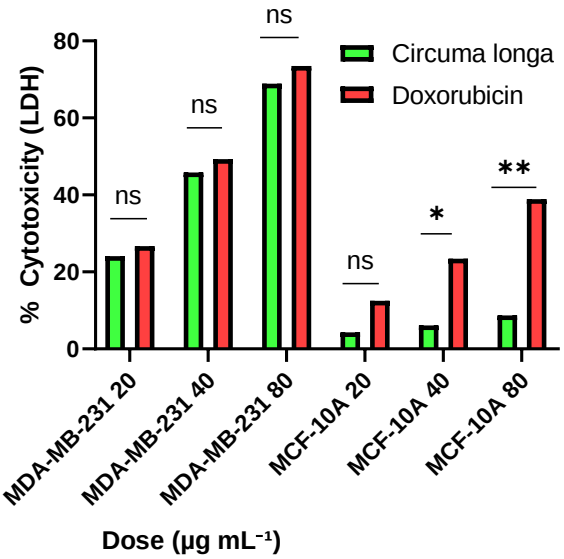


Fig. 9: Lactate dehydrogenase release in MDA-MB-231 and MCF-10A cells following treatment with *Curcuma longa* extract or doxorubicin. Cells were treated with CL extract or DOX at 20, 40 and 80 µg mL^{-1} for 24 h.

Article in Press

Cytotoxicity was calculated from LDH release and expressed as a percentage of the maximum-release control. Bars represent mean ± SD from three independent experiments (n=3). Statistical significance between CL and DOX at matched concentrations is indicated as ns, not significant; *p<0.05; and **p<0.01. CL, *Curcuma longa* extract; DOX, doxorubicin; LDH, lactate dehydrogenase; SD, standard deviation.

Mitochondrial membrane potential results

After 24 h, MDA-MB-231 cells showed a dose-dependent reduction in ΔΨm following treatment with either CL extract or DOX. CL extract produced greater mitochondrial depolarisation than DOX at matched concentrations; at 80 µg mL⁻¹, the ΔΨm ratios were 0.36 ± 0.02 and 0.42 ± 0.02 for CL extract and DOX, respectively. In MCF-10A cells, ΔΨm remained close to 1.00 across the tested CL concentrations, whereas DOX produced progressive mitochondrial depolarisation, particularly at 40 and 80 µg mL⁻¹, with ratios of 0.89 ± 0.02 and 0.80 ± 0.02, respectively. These findings indicate a greater effect of CL extract on mitochondrial depolarisation in MDA-MB-231 cells while showing minimal effect on MCF-10A cells under the tested conditions (Fig. 10).

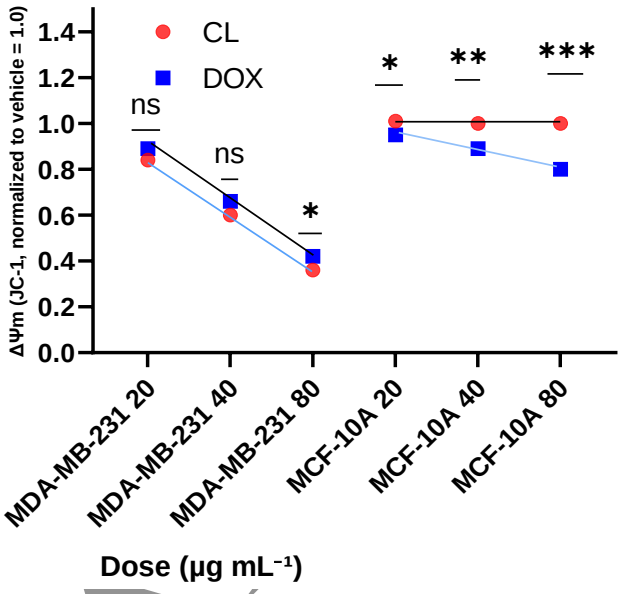


Fig. 20: Effect of *Curcuma longa* extract and doxorubicin on mitochondrial membrane potential in MDA-MB-231 and MCF-10A cells. Cells were treated with CL extract or DOX at 20, 40 and 80 µg mL⁻¹ for 24 h. Mitochondrial membrane potential was determined by JC-1 staining and expressed as the red-to-green fluorescence ratio normalised to the matched vehicle control. A lower ratio indicates greater mitochondrial depolarisation. Data are presented as mean ± SD from three independent experiments (n=3). ns, not significant; *p<0.05; **p<0.01; ***p<0.001. CL, *Curcuma longa* extract; DOX, doxorubicin; JC-1, 5,5′,6,6′-tetrachloro-1,1′,3,3′-tetraethylbenzimidazolylcarbocyanine iodide; ΔΨm, mitochondrial membrane potential; SD, standard deviation.

Caspase-3/7 and caspase-9 assay results

After 24 h, MDA-MB-231 cells showed dose-dependent increases in caspase-3/7 and caspase-9 activities following treatment with both CL extract and DOX. CL extract produced greater caspase activity than DOX at matched concentrations. At 80 µg mL⁻¹, caspase-3/7 activity was 4.08 ± 0.09 with CL extract compared with 3.37 ± 0.13 with DOX, while caspase-9 activity was 3.52 ± 0.09 and 2.95 ± 0.08, respectively. In MCF-10A cells, caspase activities remained close to baseline following CL treatment across all tested concentrations, whereas DOX produced a mild dose-dependent increase, particularly at 80 µg mL⁻¹. These findings indicate that CL extract produced greater activation of caspase-mediated apoptotic pathways in MDA-MB-231 cells while showing minimal effects in MCF-10A cells, consistent with the LDH and ΔΨm findings (Fig. 11).

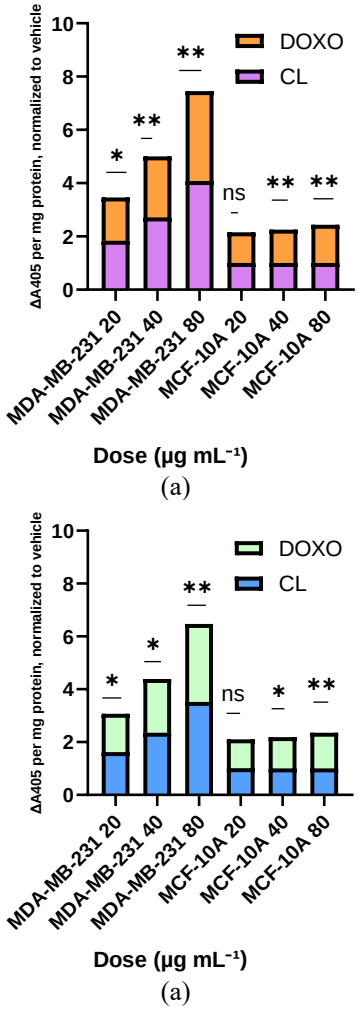


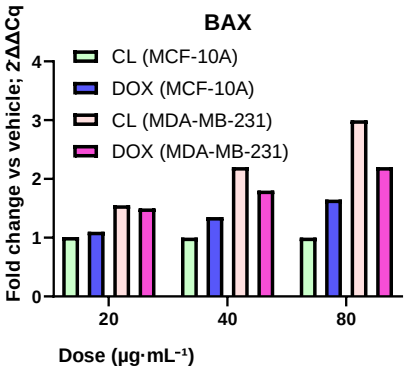
Fig. 31: Effect of *Curcuma longa* extract and doxorubicin on caspase activity in MDA-MB-231 and MCF-10A cells. Panels show the activity of (a) caspase-3/7 and (b) caspase-

In Press
Accepted

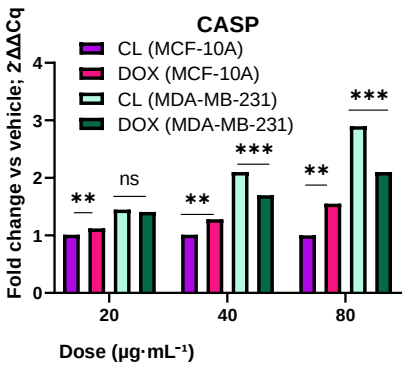
9 after treatment with CL extract or DOX at 20, 40 and 80 µg mL⁻¹ for 24 h. Caspase activity was measured at 405 nm, normalised to protein content and expressed relative to the matched vehicle control. Data are presented as mean ± SD from three independent experiments (n=3). ns, not significant; *p<0.05; **p<0.01. CL, *Curcuma longa* extract; DOX, doxorubicin; SD, standard deviation.

RT-qPCR results

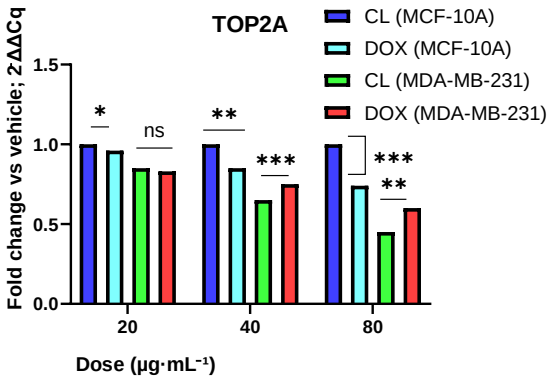
After 24 h, MDA-MB-231 cells showed dose-dependent transcriptional changes following treatment with both CL extract and DOX. At 20 µg mL⁻¹, the responses to CL extract and DOX were comparable for *BAX*, *BCL2*, *CASP9* and *TOP2A*. At 40 and 80 µg mL⁻¹, CL extract produced significantly greater up-regulation of *BAX* and *CASP9* ($p \leq 0.001$), greater down-regulation of *BCL2* ($p \leq 0.002$) and a greater reduction in *TOP2A* expression ($p \leq 0.001$) than DOX. At 20 µg mL⁻¹, differences between CL extract and DOX were not significant for most targets. In MCF-10A cells, CL extract produced minimal changes in the expression of all four transcripts, with mean values remaining close to 1.0 across the tested concentrations. In contrast, DOX produced dose-dependent increases in *BAX* and *CASP9* expression and reductions in *BCL2* and *TOP2A* expression, with significant changes observed mainly at 40 and 80 µg mL⁻¹. These transcriptional findings were consistent with the LDH, ΔΨm and caspase activity results and support a more cancer-selective apoptotic response to CL extract at higher concentrations (Fig. 12).



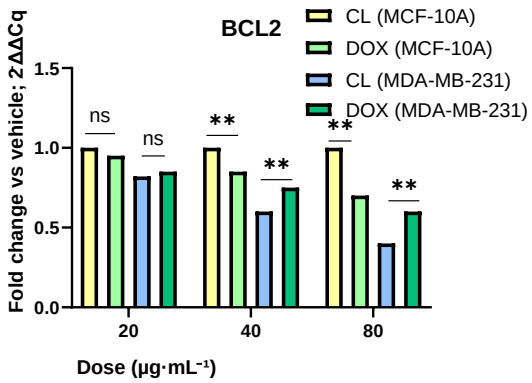
(a)



(b)



(c)



(d)

Fig. 42: Reverse transcription quantitative polymerase chain reaction analysis of apoptosis- and proliferation-related gene expression in MDA-MB-231 and MCF-10A cells following 24 h exposure to *Curcuma longa* extract or doxorubicin. Panels show the relative expression of (a) BAX; (b) CASP9; (c) TOP2A and; (d) BCL2 following treatment with 20, 40 or 80 µg mL⁻¹ CL extract or DOX. Gene expression was normalised to GAPDH and calculated relative to the matched vehicle control using the $2^{-}\Delta\Delta Cq$ method. Bars represent mean ± SD from three independent experiments (n=3). Comparisons between CL and DOX at matched concentrations were performed using two-way analysis of variance followed by Sidak's multiple-comparison test. ns, not significant; *p<0.05; **p<0.01; ***p<0.001.

DISCUSSION

The present study shows that the DCM extract of CL produces selective cytotoxicity against MDA-MB-231 breast cancer cells while showing limited toxicity toward MCF-10A non-tumourigenic mammary epithelial cells. This effect was supported by multiple experimental findings, including reduced cell viability, increased LDH release in cancer cells, ROS generation, loss of ΔΨm, caspase activation and apoptosis-related transcriptional changes. Collectively, these findings support the involvement of a coordinated intrinsic apoptotic response

rather than a reduction in cell viability alone. This finding is relevant because breast cancer treatment remains limited by drug resistance and systemic toxicity and agents showing greater cancer-cell selectivity remain pharmacologically important (Tufail *et al*., 2022; Lyon *et al*., 2022).

The cytotoxic effect observed in MDA-MB-231 cells is consistent with previous evidence that turmeric-derived constituents and other natural products can suppress cancer cell growth through induction of apoptosis, modulation of oxidative stress and regulation of the cell cycle (Ko and Moon, 2015; Ye *et al*., 2012). Curcumin has also been reported to regulate multiple molecular targets involved in cancer cell survival, proliferation and apoptosis, supporting the mechanistic relevance of the present findings (Ye *et al*., 2012). In the present study, CL produced a dose-dependent decrease in MDA-MB-231 cell viability, accompanied by morphological changes including cell shrinkage, rounding, detachment and membrane blebbing. These morphological findings were consistent with apoptosis-associated cellular changes.

The selective behaviour of CL toward cancer cells was one of the important findings of this study. MCF-10A cells remained close to baseline following CL exposure, whereas DOX produced clear toxicity in the same non-tumourigenic cell line. A similar cancer-selective pattern has been reported for *Luffa cylindrica* leaf extract, which reduced breast cancer cell viability while showing limited toxicity toward MCF-10A cells compared with DOX (Arshad and Saleem, 2025). The present findings therefore support the possibility that selected plant-derived extracts may exhibit a more favourable *in-vitro* selectivity profile than conventional cytotoxic drugs. However, this interpretation should remain limited to *in-vitro* conditions until protein-level, animal and pharmacokinetic studies are available.

ROS generation appears to be an important event in the response to CL. The extract produced a marked increase in intracellular ROS in MDA-MB-231 cells, whereas MCF-10A cells showed minimal changes. This cancer-selective oxidative stress response is consistent with the findings of Abdulazeez *et al*. (2022), who reported that *Peristrophe bicalyculata* induced oxidative stress, mitochondrial depolarisation, DNA damage and caspase-mediated intrinsic apoptosis in cancer cells. A similar relationship between oxidative stress and mitochondrial apoptosis was reported for xanthatin in ovarian cancer, where increased ROS, loss of ΔΨm and caspase activation supported a multi-target pro-apoptotic mechanism (Arshad and Afridi, 2025). These comparisons support the interpretation that ROS generation in the present study may be associated with subsequent mitochondrial injury and caspase activation.

Mitochondrial involvement was further supported by the JC-1 and caspase assay results. CL caused a dose-dependent reduction in ΔΨm in MDA-MB-231 cells, accompanied by increased caspase-9 and caspase-3/7 activities. Caspase-9 activation supports involvement of the intrinsic mitochondrial apoptotic pathway, whereas caspase-3/7 activation reflects execution-phase apoptosis. This interpretation was further supported by the gene-expression findings, in which CL up-regulated *BAX* and *CASP9* and down-regulated *BCL2*. Previous studies have shown that curcumin can regulate BCL2 family-mediated apoptosis in breast cancer models (Zhou *et al*., 2017). The present findings are consistent with this mechanism because an increased BAX/BCL2 balance favours mitochondrial outer membrane permeabilisation, subsequent caspase activation and apoptotic progression.

The transcriptional findings also suggest an antiproliferative effect of CL. CL reduced *TOP2A* expression in MDA-MB-231 cells, particularly at higher concentrations. *TOP2A* is relevant because it is associated with DNA topology, cellular proliferation and anthracycline-related mechanisms. DOX is a clinically relevant comparator because its anticancer activity includes topoisomerase II-related DNA damage, although its clinical use is limited by systemic toxicity and cardiotoxicity (Lyon *et al*., 2022). The greater reduction in *TOP2A* expression following CL treatment at higher concentrations may indicate an additional antiproliferative mechanism. However, *TOP2A* was evaluated only at the messenger RNA level; therefore, protein expression and enzyme activity require confirmation before stronger mechanistic conclusions can be made.

The chemical characterisation findings provide a basis for interpreting the biological activity of CL. HPLC, LC-MS and FT-IR analyses identified curcuminoid-related constituents, including curcumin, demethoxycurcumin and bisdemethoxycurcumin. Vardhini *et al*. (2023) also reported the purification and characterisation of curcumin, desmethoxycurcumin and bisdemethoxycurcumin from *Curcuma longa*, supporting the relevance of these compounds as major bioactive markers. Abualhasan *et al*. (2023) similarly reported chromatographic characterisation and anticancer activity of *Curcuma longa* extract, further supporting the association between chemical composition and cytotoxic potential. Nadeem *et al*. (2025) and Nahar *et al*. (2025) also support the value of combining phytochemical profiling with biological evaluation in natural-product research.

The comparison with DOX adds translational relevance to the study. CL produced responses comparable to or greater than those of DOX in MDA-MB-231 cells at higher concentrations while producing considerably smaller effects in MCF-10A cells. This pattern suggests that CL may serve as a source of active anticancer constituents or

Article in Press

as a candidate for future combination studies with anthracyclines. The qualitative solubility findings were also consistent with the chemical characteristics of the extract. CL extract was soluble in chloroform, acetone, ethanol and methanol but insoluble in distilled water. This solvent-dependent behaviour may be attributed primarily to the hydrophobic nature of curcuminoids, which show poor aqueous solubility but improved dissolution in several organic solvents (Górnicka *et al*., 2023; Slaček *et al*., 2023). Comparative analysis of *Curcuma longa* extracts has similarly shown that organic solvents, including DCM, acetone, methanol and ethanol, recover more curcuminoid-rich material than water (Moulick *et al*., 2025). Poor aqueous solubility remains an important limitation for biological delivery and should be addressed in future studies through extract standardisation and suitable solubilisation or formulation strategies. Therefore, further work should first focus on standardising the extract, identifying its active fractions and improving delivery before therapeutic claims are considered.

The study has several limitations. First, the use of a crude DCM extract prevents attribution of the observed activity to a single constituent and may introduce batch-to-batch variation. Second, although multiple complementary assays were used, several findings remain indirect or semi-quantitative. Annexin V/PI and Hoechst 33342/PI staining would be strengthened by flow-cytometric quantification. Third, the proposed apoptotic mechanism was supported by caspase activity and gene expression findings, but protein-level validation by Western blotting for cleaved caspase-3, BAX, BCL2 and TOP2A was not performed. Fourth, only two cell lines were included, limiting generalisability across different breast cancer subtypes. Fifth, the study used a 24-h exposure period and time-course experiments are needed to distinguish early ROS generation, mitochondrial injury, apoptosis and secondary necrosis. Finally, *in-vivo* pharmacokinetic, toxicity and efficacy data are not available; therefore, the current findings should be interpreted as preclinical *in-vitro* evidence only.

Future studies should focus on bioactivity-guided fractionation to identify the most active constituents of CL. Active fractions should then be evaluated across a broader panel of breast cancer cell lines and in patient-derived models. Protein-level confirmation of BAX, BCL2, cleaved caspase-3, cleaved caspase-9 and TOP2A should also be performed. Flow cytometry should be used to quantify early apoptosis, late apoptosis and necrosis. Combination studies with DOX are warranted to determine whether CL or its active fractions can reduce the required DOX dose while maintaining anticancer activity. Finally, *in-vivo* efficacy, pharmacokinetic and toxicity studies are required before therapeutic claims can be made. Overall, the present study supports the hypothesis that CL induces cancer-selective apoptosis in MDA-MB-231 breast cancer cells through oxidative stress, mitochondrial depolarisation, caspase activation and apoptosis-related transcriptional regulation. The limited response observed in MCF-10A cells suggests a favourable *in-vitro* selectivity profile. These findings support further standardisation, fractionation and mechanistic validation of CL as a potential source of anticancer lead compounds.

CONCLUSION

The DCM extract of CL exhibited selective anticancer activity against MDA-MB-231 cells via oxidative stress, mitochondrial depolarisation and caspase-mediated apoptosis, while showing limited toxicity toward MCF-10A cells. Further mechanistic and *in-vivo* studies are required before its therapeutic potential can be established.

Acknowledgment
None.

Authors' contributions
HA conceived and designed the study, performed the experimental work, analysed the data and drafted the manuscript; IUR provided academic supervision, reviewed the manuscript and approved the final version for submission; MM contributed to experimental work, data collection and manuscript review; AM contributed to extract preparation, laboratory work and manuscript review; ARR contributed to data organisation, figure preparation and manuscript revision; SUK guided the methodology and critically revised the manuscript. All authors read and approved the final manuscript.

Funding
There was no funding.

Data availability statement
The datasets generated during and/or analysed during the current study are available from the corresponding author on reasonable request.

Ethical approval
Not applicable.

Conflict of interest
The authors declare no conflict of interest.

REFERENCES

Abdulazeez MA, Jasim HA, Bashir M, Ross K and Fatokun AA (2022). *Peristrophe bicalyculata* (Retz) Nees contains compounds that are cytotoxic to cancer cells and induce caspase-mediated intrinsic apoptotic death through oxidative stress, mitochondrial depolarisation and DNA damage. *Biomed. Pharmacother.*, **147**: 112597.

Article in Press

Abualhasan M, Jaradat N, Hawash M, Shraim N, Asaad M, Mousa A, Mousa Z, Tobeh R and Mlitat B (2023). Chromatographic analysis of the chemical composition and anticancer activities of *Curcuma longa* extract cultivated in Palestine. *Open Life Sci.*, **18**(1): 20220767.

Altundağ EM, Ustürk S, Özbilenler C and Yılmaz AM (2025). Chemical characterization, antioxidant potential and cytotoxicity of *Bougainvillea spectabilis* Willd. flowers cultivated in northern Cyprus. *Sci. Rep.*, **15**: 38056.

American Type Culture Collection (2026a). MCF 10A, CRL-10317. Available at: https://www.atcc.org/products/crl-10317 (Accessed 27 July 2026).

American Type Culture Collection (2026b). MDA-MB-231, HTB-26. Available at: https://www.atcc.org/products/htb-26 (Accessed 27 July 2026).

Arshad H and Afridi MSK (2025). Experimental and computational evidence for xanthatin as a multi-target anticancer agent in ovarian cancer. *Bangladesh J. Pharmacol.*, **20**(4): 158-168.

Arshad H and Saleem M (2025). Cytotoxic effect of *Luffa cylindrica* leaf extract on MCF-7 cell lines. *Bangladesh J. Pharmacol.*, **20**(3): 101-112.

Azwanida NN (2015). A review on the extraction methods use in medicinal plants, principle, strength and limitation. *Med. Aromat. Plants*, **4**(3): 196.

Bray F, Laversanne M, Sung H, Ferlay J, Siegel RL, Soerjomataram I and Jemal A (2024). Global cancer statistics 2022: GLOBOCAN estimates of incidence and mortality worldwide for 36 cancers in 185 countries. *CA Cancer J. Clin.*, **74**(3): 229-263.

Cellosaurus (2026a). Cell line MCF-10A (CVCL_0598). Available at: https://www.cellosaurus.org/CVCL_0598 (Accessed 27 July 2026).

Cellosaurus (2026b). Cell line MDA-MB-231 (CVCL_0062). Available at: https://www.cellosaurus.org/CVCL_0062 (Accessed 27 July 2026).

Daina A, Michielin O and Zoete V (2017). SwissADME: A free web tool to evaluate pharmacokinetics, drug-likeness and medicinal chemistry friendliness of small molecules. *Sci. Rep.*, **7**: 42717.

Daina A, Michielin O and Zoete V (2019). SwissTargetPrediction: Updated data and new features for efficient prediction of protein targets of small molecules. *Nucleic Acids Res.*, **47**(W1): W357-W364.

Decker T and Lohmann-Matthes ML (1988). A quick and simple method for the quantitation of lactate dehydrogenase release in measurements of cellular cytotoxicity and tumour necrosis factor activity. *J. Immunol. Methods*, **115**(1): 61-69.

Eberhardt J, Santos-Martins D, Tillack AF and Forli S (2021). AutoDock Vina 1.2.0: New docking methods, expanded force field and Python bindings. *J. Chem. Inf. Model.*, **61**(8): 3891-3898.

Eruslanov E and Kusmartsev S (2010). Identification of reactive oxygen species using oxidized DCFDA and flow cytometry. *Methods Mol. Biol.*, **594**: 57-72.

Freshney RI (2010). Subculture and cell lines. In: Freshney RI (ed.), *Culture of Animal Cells: A Manual of Basic Technique and Specialized Applications*, 6th ed., Wiley-Blackwell, Hoboken, pp. 187-206.

Górnicka J, Mika M, Wróblewska O, Siudem P and Paradowska K (2023). Methods to improve the solubility of curcumin from turmeric. *Life*, **13**(1): 207.

Kafeel S, Inam-ur-Raheem M, Khan MR and Faisal MN (2023). Phytochemical characterisation and antioxidant capacities of pomegranate peel. *Int. J. Food Sci. Technol.*, **58**(9): 4543-4550.

Ko EY and Moon A (2015). Natural products for chemoprevention of breast cancer. *J. Cancer Prev.*, **20**(4): 223-231.

Krysko DV, Vanden Berghe T, D'Herde K and Vandenabeele P (2008). Apoptosis and necrosis: Detection, discrimination and phagocytosis. *Methods*, **44**(3): 205-221.

Liang CC, Park AY and Guan JL (2007). *In-vitro* scratch assay: A convenient and inexpensive method for analysis of cell migration *in-vitro*. *Nat. Protoc.*, **2**(2): 329-333.

Livak KJ and Schmittgen TD (2001). Analysis of relative gene expression data using real-time quantitative PCR and the $2^{-}\Delta\Delta CT$ method. *Methods*, **25**(4): 402-408.

Lyon AR, López-Fernández T, Couch LS, Asteggiano R, Aznar MC, Bergler-Klein J, Boriani G, Cardinale D, Córdoba R, Cosyns B, Cutter DJ, de Azambuja E, de Boer RA, Dent SF, Farmakis D, Gevaert SA, Gorog DA, Herrmann J, Lenihan D, Moslehi J, Moura B, Salinger SS, Stephens R, Suter TM, Szmit S, Tamargo J, Thavendiranathan P, Tocchetti CG, van der Meer P, van der Pal HJH and ESC Scientific Document Group (2022). 2022 ESC Guidelines on cardio-oncology developed in collaboration with the European Hematology Association, the European Society for Therapeutic Radiology and Oncology and the International Cardio-Oncology Society. *Eur. Heart J. Cardiovasc. Imaging*, **23**(10): e333-e465.

Moulick SP, Al Bashera M, Jahan F, Uddin MN, Rana GMM, Islam MB, Islam F, Hasan MS, Ahmed S and Boby F (2025). Turmeric (*Curcuma longa* L.) extract in different solvents: A comparative study of curcuminoid content, volatile compounds and antimicrobial activity with molecular docking insights. *Food Chem. Adv.*, **8**: 101074.

Nadeem M, Zarreen F and Rizvi MMA (2025). GC-MS analysis of phytochemical composition and anticancer activities of methanol and aqueous extracts of *Bergenia ligulata* rhizome. *J. Food Sci. Technol.*, **62**: 623-634.

Nahar A, Khandakar MJ, Mamun MJI, Rasel MH, Ihsan AB, Raj A, Ahmed S, Hossain MK, Hasan MR and Saito T (2025). Investigation of analgesic, anti-inflammatory and thrombolytic effects of methanolic extract and its

Article in Press

fractions of *Dischidia bengalensis*: *In-vitro* and *in-vivo* studies with *in-silico* interventions. *Molecules*, **30**(18): 3724.

National Center for Biotechnology Information (2026). PubChem. Available at: https://pubchem.ncbi.nlm.nih.gov/ (Accessed 27 July 2026).

Pires DEV, Blundell TL and Ascher DB (2015). pkCSM: Predicting small-molecule pharmacokinetic and toxicity properties using graph-based signatures. *J. Med. Chem.*, **58**(9): 4066-4072.

RCSB Protein Data Bank (2026). RCSB Protein Data Bank. Available at: https://www.rcsb.org/ (Accessed 27 July 2026).

Ribble D, Goldstein NB, Norris DA and Shellman YG (2005). A simple technique for quantifying apoptosis in 96-well plates. *BMC Biotechnol.*, **5**: 12.

Silverstein RM, Webster FX, Kiemle DJ and Bryce DL (2014). Infrared spectrometry. In: *Spectrometric Identification of Organic Compounds*, 8th ed., John Wiley & Sons, Hoboken, pp. 95-137.

Slaček G, Kotnik P, Osmić A, Postružnik V, Knez Ž, Finšgar M and Knez Marevci M (2023). The extraction process, separation and identification of curcuminoids from turmeric *Curcuma longa*. *Foods*, **12**(21): 4000.

Smith PK, Krohn RI, Hermanson GT, Mallia AK, Gartner FH, Provenzano MD, Fujimoto EK, Goeke NM, Olson BJ and Klenk DC (1985). Measurement of protein using bicinchoninic acid. *Anal. Biochem.*, **150**(1): 76-85.

Strober W (2015). Trypan blue exclusion test of cell viability. *Curr. Protoc. Immunol.*, **111**: A3.B.1-A3.B.3.

Swiss Institute of Bioinformatics (2026a). SwissADME. Available at: https://www.swissadme.ch/ (Accessed 27 July 2026).

Swiss Institute of Bioinformatics (2026b). SwissTargetPrediction. Available at: https://www.swisstargetprediction.ch/ (Accessed 27 July 2026).

Thornberry NA, Rano TA, Peterson EP, Rasper DM, Timkey T, Garcia-Calvo M, Houtzager VM, Nordstrom PA, Roy S, Vaillancourt JP, Chapman KT and Nicholson DW (1997). A combinatorial approach defines specificities of members of the caspase family and granzyme B. *J. Biol. Chem.*, **272**(29): 17907-17911.

Tufail M, Cui J and Wu C (2022). Breast cancer: Molecular mechanisms of underlying resistance and therapeutic approaches. *Am. J. Cancer Res.*, **12**(7): 2920-2949.

Vardhini NM, Punia J, Jat S, Pawar SD, Devi N, Radhakrishnanand P, Murty USN, Saini A, Sethi KK and Kumar P (2023). Purification and characterization of pure curcumin, desmethoxycurcumin and bisdemethoxycurcumin from North-East India Lakadong turmeric (*Curcuma longa*). *J. Chromatogr. A*, **1708**: 464358.

Vermes I, Haanen C, Steffens-Nakken H and Reutelingsperger C (1995). A novel assay for apoptosis: Flow cytometric detection of phosphatidylserine expression on early apoptotic cells using fluorescein-labelled Annexin V. *J. Immunol. Methods*, **184**(1): 39-51.

Wang H and Joseph JA (1999). Quantifying cellular oxidative stress by dichlorofluorescein assay using microplate reader. *Free Radic. Biol. Med.*, **27**(5-6): 612-616.

Ye MX, Li Y, Yin H and Zhang J (2012). Curcumin: Updated molecular mechanisms and intervention targets in human lung cancer. *Int. J. Mol. Sci.*, **13**(3): 3959-3978.

Zhou QM, Sun Y, Lu YY, Zhang H, Chen QL and Su SB (2017). Curcumin reduces mitomycin C resistance in breast cancer stem cells by regulating Bcl-2 family-mediated apoptosis. *Cancer Cell Int.*, **17**: 84.

Article in Press